Revised version

Evidence of multi-phase Cretaceous to Quaternary alkaline magmatism on Tore-Madeira Rise and neighbouring seamounts from $^{40}Ar/^{39}Ar$ ages

Renaud Merle[a]*, Fred Jourdan[b,c], Andrea Marzoli[a], Paul R. Renne[b,d], Marion Grange[e], Jacques Girardeau[f]

[a] Dipartimento de Geoscienze, Universita di Padova, Via Giotto 1, 35137 Padova, Italia.

[b] Berkeley Geochronology Center, 2455 Ridge Road, Berkeley, CA 94709, USA.

[c] Western Australian Argon Isotope Facility, Department of Applied Geology and JdL-CMS, Curtin University of Technology, G.P.O. Box U1987, Perth, Western Australia 6845, Australia.

[d] Department of Earth and Planetary Science, University of California, Berkeley, California, 94720, USA

[e] Department of Applied Geology, Curtin University of Technology, G.P.O. Box U1987, Perth, Western Australia 6845, Australia.

[f] Laboratoire de Planétologie et Géodynamique, UMR-CNRS 6112, Université de Nantes, 2 rue de la Houssinère, 44322 Nantes cedex 3, France.

*Corresponding author.
Now at University of Western Australia, School of Earth and Geographical Sciences, 35 Stirling Highway Crawley, WA 6009, Australia.
Phone: +61 8 64882666. Fax: +61 8 64881037
E-mail : rmerle@cyllene.uwa.edu.au

7732 Words, 64 references, 10 figures, 4 tables

Abstract

The Tore-Madeira Rise (TMR) is a seamounts chain located 300 km off the Portugal and Morocco coasts attributed to a hot-spot activity. U-Pb ages of lavas from the northern and central TMR range between 103 and 80.5 Ma while $^{40}Ar/^{39}Ar$ ages from central and southern TMR yield ages ranging from 94.5 to 0.5 Ma. We performed new $^{40}Ar/^{39}Ar$ measurements in order to better understand the geodynamic history of the TMR. Plagioclase ages from Bikini Bottom and Torillon seamounts suggest ages of >90 Ma and ≥60 Ma respectively. Amphiboles from Seine seamount yield an age of 24.0 ± 0.8 Ma. Biotites from lavas of Ashton seamount give ages of 97.4 ± 1.1 Ma and 97.8 ± 1.1 Ma. The geochronological database available on TMR has been filtered on statistical criteria to eliminate unreliable ages. The resulting database reveals 3 pulses of alkaline magmatism on TMR at 103-80.5 Ma, at ~68 Ma and between 30 Ma to Present. The magmatism was continuous from 103 until ~68 Ma and from ~30 Ma until Present on the TMR, the surrounding seamounts and the Portuguese cost. We suggest that the space-time distribution of this magmatism results from the interaction between a wide thermal anomaly emitting magmatic pulses and the complex motion of the Iberian plate.

Supplementary material: Detailed Ar measurements data set is available at http://www.geolsoc.org.uk

The Tore-Madeira Rise (TMR) is a 1000 km long by 50 km wide seamount chain, oriented NNE-SSW along the Atlantic coast of Portugal and Morocco (Fig. 1a). It includes a dozen seamounts extending from the Tore seamount, located 300 km west of Lisbon, to the Madeira archipelago. For several decades, the nature of the rocks forming this aseismic ridge was almost unknown, and only very few samples were available. Two dredging campaigns were carried out in 2001 (R/V Meteor expedition M51/1; Tore-Madeira Rise cruise, R/V *Atalante*) to constrain the age and the main chemical characteristics of the rocks constituting the rise and to decipher the geodynamical process leading to the construction of the TMR. Abundant alkaline lavas displaying similar chemical characteristics were dredged along the whole rise in addition to surrounding alkaline magmatism occurrences (Fig. 1). Two sets of contrasting ages were obtained on lavas from seamounts along the whole rise. Titanite and zircon U-Pb ages from differentiated lavas of the northern and central part of the rise ranged between ~104 and ~80 Ma (Merle et al., 2006); $^{40}Ar/^{39}Ar$ measurements carried out on groundmass and mineral separates from central and southern TMR seamounts yielded Cretaceous (94 Ma) to Pleistocene ages (Geldmacher et al., 2005, 2006, 2008). All these studies argue for a hot-spot as the source of the TMR but it is still unclear if the TMR magmatism was related to the Madeira and/or Canary plumes (Geldmacher et al., 2006) or to a deep rooted thermal anomaly feeding the Azores, Madeira and Canaries hot-spots (Merle et al., 2006). Alternative hypotheses are accretion-related off-axis magmatic activity (Jagoutz et al., 2007) or shallow mantle upwelling (Geldmacher et al., 2008). These hypotheses are however closely dependent on the reliability of the ages of the various seamounts. Moreover, no ages are available for some seamounts, in particular those located slightly off the main TMR alignment. As a consequence, the geodynamic process that triggered the magmatism on the TMR and the surrounding area is still debated and additional geochronological data are required for the entire area.

The aim of this work is to document new $^{40}Ar/^{39}Ar$ dating performed on plagioclase, biotite and amphibole separates from lavas of four seamounts to improve the reliability of the two contrasting age sets mentioned previously. New and carefully selected published ages, and geochemical and isotopic data are discussed and combined together to obtain a more complete overview of the construction of the Tore-Madeira Rise. We give a new geodynamic interpretation of the TMR and the magmatic occurrences of this part of the Atlantic Ocean.

Geological setting

The Tore-Madeira Rise (TMR) ranges roughly from 40°20'N to 32°30'N and from 11°30'W to 17°40'W. It displays a NNE-SSW trending alignment of mounts which is surrounded by scattered seamounts (Fig. 1a). The northern limit of the rise is the ~2500 m high Tore seamount which rims an elliptic (120 km by 90 km) depression lying at 5000 m below sea level. The scattered seamounts occurring in the vicinity of the main alignment are the Bikini Bottom seamount, located to the NNW of Tore; Torillon, lying at around 100 km on the WSW of Tore; Unicorn and Seine seamounts (Fig. 1b). Most of the seamounts are at least 30 km in diameter (Seine reaches 48 km) for a height of over 3000 m above sea floor. Considering the dimension of the TMR (1000 km long by 50 km wide, 2 km high), the estimated volume of magma emitted could reach 10^5 km^3. The TMR has been considered as one of the main structures in the Northern Central Atlantic ocean.

The Azores-Gibraltar Fracture Zone (AGFZ), separating the Eurasian and African plates, is an important Atlantic transform fault which splits into three branches towards the Tore seamounts, Gorringe Bank, and Ampere-Coral Patch seamounts (e.g., Laughton et al., 1975; Jiménez-Munt et al., 2001; Fig. 1). Since Oligocene times, movements along the branches of the AGFZ seem to be transpressive, with a slight dextral component (Le Gall et

al., 1997; Malod, personal comm.) while movements were very limited from Early Jurassic to Oligocene times (Olivet, 1996).

Seamounts to the North of the AGFZ lie along the J anomaly which is the first magnetic anomaly created by the Atlantic spreading centre along the Iberia margin (M0 to M3 magnetic anomalies, 125-130 Ma; Gradstein et al., 2004; Fig.1b). This anomaly corresponds to the boundary between true oceanic crust and a transitional domain composed of continental lithosphere peridotites exhumed during rifting and stretching of the Iberian margin (Boillot et al., 1989; Beslier et al., 1993; Girardeau et al., 1998). To the South beyond the central branch of the AGFZ, magnetic anomalies older than J seem to be present in the Seine Abyssal Plain (Roest et al., 1992) implying that some seamounts of the TMR could be emplaced onto oceanic lithosphere.

The geodynamical process leading to the construction of the TMR is still debated. Several explanations were put forward such as a hot-spot probably active coevally with spreading (Tucholke and Ludwig, 1982; Pierce and Barton, 1991; Geldmacher et al., 2006; Merle et al., 2006), accretion-related off-axis magmatic activity (Jagoutz et al., 2007) or shallow mantle upwelling (Geldmacher et al., 2008). It has been proposed that the TMR was built up by two magmatic phases, the earliest during Cretaceous times (Merle et al., 2006) constituting the basement of the rise capped by late Tertiary to recent magmas (Geldmacher et al., 2006). The magmas may have been focused along the lithospheric discontinuities which facilitated the magma ascent through the lithosphere (van der Linden, 1979; Geldmacher et al., 2006; Merle et al., 2006).

In the neighbouring region of the TMR (within < 1000 km; Fig. 1b), widespread alkaline magmatism occurs on Ormonde seamount (62-68 Ma, $^{40}Ar/^{39}Ar$ ages on both matrix and minerals; Féraud et al., 1982; 1986); Ampère-Coral Patch seamounts (~31 Ma, $^{40}Ar/^{39}Ar$ ages on whole-rock samples; Geldmacher et al., 2000) and on the continent (Serra de

Monchique complex: 69-70 Ma; Sines complex: 73-77 Ma; Sintra complex: 80-83 Ma; and Ribamar intrusion: ~88 Ma; U-Pb ages on titanite and zircon; Grange et al., 2007). All these magmatic occurrences as well as TMR samples display OIB-like geochemical characteristics, the specific positive Nb anomaly, in particular (Bernard-Griffith et al., 1997; Geldmacher et al., 2006; 2008; Merle, 2006). The isotopic characteristics of the TMR rocks and the surrounding alkaline occurrences are interpreted to be derived from the same OIB-type (mantle plume-like) source (Geldmacher and Hoernle, 2000; Geldmacher et al., 2006; Merle et al., 2006). However, isotopic heterogeneities exist between the different seamounts and within the same edifice. The isotopic compositions of the lavas from Godzilla seamount (Fig. 1) are clearly distinct from the compositions of the other seamounts of the TMR (see Geldmacher et al., 2006; 2008). The Cretaceous lavas display distinct isotopic characteristics from the Late Cenozoic volcanics (Geldmacher et al., 2006) and a significant variation of the isotopic signature is observed among the Seine seamount samples (Geldmacher et al., 2005).

Previous geochronological data from the TMR seamounts

As already emphasized, two datasets of contrasting ages were obtained on lavas along the whole rise (see Fig. 1b). All the previous $^{40}Ar/^{39}Ar$ measurements were performed using the Taylor Creek Rhyolite sanidine (TCRs) standard for which the authors adopted an age of 27.92 Ma (Dalrymple and Duffield, 1988; Duffield and Dalrymple, 1990). All the previous geochronological data from the TMR are given in Table A1 in online appendixes, together with analytical methods, rock types, material dated, ages with errors and standards used.

The lavas from the northern seamounts Tore, Sponge Bob and Ashton seamounts are dated by U-Pb methods on titanite and zircon from 80.5 ± 0.9 Ma to 104.4 ± 1.4 Ma (Merle et al., 2006).

In the central part of the rise, evolved lavas from Gago Coutinho seamount (also named Teresa by Geldmacher et al., 2006) have been dated between 92.3 ± 3.8 Ma and 94.5 ± 0.4 Ma (Geldmacher et al., 2006; Merle et al., 2006). Basic rocks dredged on Josephine North (Fig. 1) are dated by $^{40}Ar/^{39}Ar$ on whole-rock between 0.5 ± 0.1 Ma and 7.4 ± 0.5 Ma (Geldmacher et al., 2006) and those from Josephine seamount yielded ages between 8.2 ± 0.2 Ma and 15.8 ± 0.9 Ma (Wendt et al., 1976; Geldmacher et al., 2006). The basaltic rocks dredged on the Jo Sister seamount (also named Erik by Geldmacher et al., 2006) dated by $^{40}Ar/^{39}Ar$ on matrix give an age of 3.62 ± 0.32 Ma (Geldmacher et al., 2006) while the dredged evolved lavas are dated between 86.5 ± 3.4 Ma and 89.3 ± 2.3 by U-Pb on titanate (Merle et al., 2006).

Seamounts from the southern part of the TMR have been dated by $^{40}Ar/^{39}Ar$, except the altered basaltic samples dredged on Lion seamount estimated by a foraminifera fauna at ~80 Ma (Geldmacher et al., 2006). The basaltic lavas dredged on Dragon seamount are dated between 3.9 ± 0.3 Ma and 1.18 ± 0.18 Ma (Geldmacher et al., 2006) and those dredged on Seine seamount, Unicorn and Godzilla seamounts yield $^{40}Ar/^{39}Ar$ ages of 21.7 ± 0.2 Ma, 27.4 ± 2.4 Ma and around 66 Ma respectively (Geldmacher et al., 2005; 2008).

The $^{40}Ar/^{39}Ar$ ages of whole rock and separated plagioclase grains from the Madeira archipelago lavas range from 14.3 ± 0.2 Ma to 0.2 ± 0.1 Ma (Geldmacher et al., 2000 and references therein).

Analytical procedures

Mineral and whole rock analyses

Electron microprobe analyses (EMPA) of magmatic phases were performed with a Cameca SX50 automated electron microprobe (Microsonde Ouest, Brest), using an acceleration voltage of 15 kV, a beam current of 15 nA, a counting time of 6 s and correction by the ZAF method. Concentrations of < 0.3 Wt % are considered qualitative. Major and trace element analyses were carried out by ICP-AES and ICP-MS at the University of Brest and the CRPG at Nancy (analytical procedures in Govindaraju and Mevelle, 1987 and Carignan et al., 2001). For the samples analysed at University of Brest, specific details for the analytical methods and sample preparation can be found in Cotten et al., 1995.

$^{40}Ar/^{39}Ar$ geochronology

Plagioclases were separated from either the 100-200 μm or the 200-315 μm fractions using a Frantz isodynamic magnetic separator. The plagioclases recovered in the 2 Amperes non-magnetic fraction were selected by grain-by-grain hand-picking under the binocular microscope. The amphibole and biotite grains were separated using heavy liquids (CH_3Br_3 and CH_2I_2 respectively) and were hand-picked using a binocular microscope. Plagioclase and amphibole were further leached using diluted HF (2N) for 5 minutes and thoroughly rinsed in distilled water. The samples were loaded into aluminium discs along with the Fish Canyon sanidine standard (FCs = 28.03 ± 0.08 Ma, Jourdan and Renne, 2007) and irradiated for 10 h in the CLICIT facility at the TRIGA reactor, Oregon.

$^{40}Ar/^{39}Ar$ analyses were performed at the Berkeley Geochronological Center. Both single-grain and multi-grain aliquots were degassed by step heating using a CO_2 laser with focused lenses and beam-integrator lens, respectively. Ar isotopes were measured in static mode using a MAP 215-50 mass-spectrometer. Mass discrimination was monitored several times a day and yields a mean D-value of 1.00633 ± 0.00175 per AMU based on a power-law

correction. Blank measurements were generally obtained after every three sample runs. *J*-values were calculated as the mean and standard deviation of the wells bracketing the samples (see for example, Jourdan and Renne, 2007) and yield a value of 0.002630 ± 0.000014 (0.54%, see online appendixes, Table A2). Ages were calculated using the decay constant recommended by Steiger and Jäger (1977) and step-heating details are given in online appendixes (Table A2) along with Ar isotopic data corrected for blank, mass discrimination and radioactive decay. Individual errors in online appendixes (Table A2) are given at 1σ level.

Our criteria for the determination of plateau ages are as follows: plateaus must include at least 70% of the ^{39}Ar released; they should be distributed over a minimum of 3 consecutive steps indistinguishable at 95% confidence level and satisfied a probability of fit of at least 0.05. Plateau ages are given at the 2σ level and are calculated using the mean of all the plateau steps, each weighted by the inverse variance of their individual analytical error. Integrated ages (2σ) are calculated using the total gas released for each Ar isotope. Inverse isochrons include the maximum number of consecutive steps with a probability of fit ≥0.05. The uncertainties on the $^{40}Ar^*/^{39}Ar^*$ ratios of the monitor are included in the calculation of the plateau age uncertainties but not the errors on the age of the monitor and on the decay constants (internal errors only).

Results

This work presents new ages for four samples dredged during the Tore-Madeira Rise cruise. They come from Bikini Bottom, Torillon, and Seine seamounts, located off the main trend of the TMR. In addition, biotites from a trachyte dredged on the Ashton seamount have also been dated to test a previous U-Pb age obtained on possibly inherited zircon grains (Merle et

al., 2006) given that Ashton seamount is located on the very edge of the continental lithosphere (Fig. 1b). Coordinates and water depths of sampling sites are given in Table 1.

Petrological notes

The EMPA of mineral phases from the TMR samples are available in online appendixes (Table A3). All but one sample (Ashton trachyte; TMD 14-9) display evidence of seawater interaction occurring as carbonate, Fe-Mn hydroxides, brown-green clays and rare zeolites (K-zeolites: phillipsite and erionite) invading the groundmass and filling cracks and vesicles. However, it is worth noting that the phenocrysts are usually well preserved. The sample from Bikini Bottom (TMD 2-1) is a slightly altered basaltic trachyandesite containing well preserved phenocrysts of abundant (30% modal) plagioclase (2-8 mm in size), rare clinopyroxene (<1 mm), Fe-Ti oxides and iddingsitized olivine (1-2 mm in size). The groundmass is composed of feldspar laths and Fe-Ti oxides grains. The basic sample from Torillon seamount (TMD 12b-1) contains phenocrysts of iddingsitized olivine and scarce well preserved plagioclase (>10 mm-size). The groundmass is composed of feldspar laths, Fe-Ti oxides grains and altered rare olivine grains. The TMD 14-9 sample is a fresh highly porphyritic trachyte containing K-feldspars subordinate biotite and sparse clinopyroxene and Fe-Ti oxides. The groundmass is composed by the same minerals (Merle et al., 2006). The detailed description of this sample can be found in Merle et al. (2006). Sample TMD 21-2 from Seine seamount is a basanite containing phenocrysts of clinopyroxene (~5% modal), iddingsitized olivine (~5% modal), microphenocrysts of Fe-Ti oxides and subordinate brown amphibole (~1% modal) reaching 4 mm-size. The groundmass is composed of feldspar laths, clinopyroxene, Fe-Ti oxides grains and olivine.

259 *Major and trace elements*

260

261 The whole-rock analyses of the samples TMD 2-1, TMD 12b-1 and TMD 21-2 are given in
262 Table 2. The sample TMD 14-9 has been documented by Merle et al. (2006). It is a very well-
263 preserved trachyte (LOI = 2 wt %) whose incompatible elements patterns display Ba, Sr and
264 Ti negative anomalies due to feldspar and Fe-Ti oxides fractionation. Apart from this sample,
265 the others show moderate to high loss on ignition (LOI = 3.0 to 11.0 wt %). Samples TMD 2-
266 1 and TMD 21-2 having less than 4.5 wt % of LOI can be more confidently plotted in the
267 TAS diagram (not shown) and plot in the field of basaltic trachy-andesite and basanite,
268 respectively. However, this result should be considered with caution since the seawater
269 alteration has probably modified the chemistry of the rocks, especially the potassium content
270 (see discussion below). All the samples documented here display steep multi-element patterns
271 with an important enrichment in the most incompatible elements (LREE, LILE, Th, Nb),
272 typical of OIB-type lavas (Fig. 2). Sample TMD 21-2 especially displays a positive Nb
273 anomaly and its pattern shows similarities relative to the previously documented Seine
274 samples (Geldmacher et al., 2005; Fig. 2). Generally, positive K and P anomalies such as
275 observed in the pattern of the TMD 12b-1 sample (Fig. 2) could correspond to feldspar and
276 apatite mineral accumulation but as neither of these minerals is observed, these anomalies are
277 more likely related to seawater interaction. The data points from the studied samples plot in
278 the field of the previously analysed TMR volcanics in the Zr/Y vs Th/Nb diagram (Fig. 3)
279 suggesting that these rocks belong to the same magmatic events as those documented by
280 Geldmacher et al. (2005, 2006).

281

282 *$^{40}Ar/^{39}Ar$ geochronology*

283

Summarized $^{40}Ar/^{39}Ar$ results are shown in Table 3.

Plagioclase analyses from TMD 2-1 (Bikini Bottom) show a U-shaped age spectrum with the oldest steps defining a weighted mean >90 Ma (Fig. 4a). The Ca/K ratio of this sample calculated from $^{37}Ar/^{39}Ar$ mimics the pattern of the age spectrum. The Ca/K of these plagioclase grains obtained by EMPA analyses is significantly higher which indicates the presence of a K-rich phase component in the $^{40}Ar/^{39}Ar$ results (Fig. 4a). These observations suggest that the plagioclase grains locally underwent partial alteration leading to recrystallization of a K-rich phase such as adularia. A minimum age of 90 Ma could be estimated upon the heating steps having the highest Ca/K (Fig. 4a). Similarly, $^{40}Ar/^{39}Ar$ measurements carried out on TMD 12b-1 (Torillon) plagioclase did not yield a plateau age (Fig. 4b). As for sample TMD 2-1, the Ca/K spectrum mimics the pattern of the age spectrum but displays only slight perturbation (Fig. 4b). The EMPA analyses yielded a mean Ca/K value well within error of the Ca/K ratio derived from the Ar experiments and suggest only negligible perturbation. Nevertheless, sample TMD 12b-1 failed to provide a plateau age and based on steps associated with the highest Ca/K ratio, can only be interpreted as a minimum age of ~60 Ma (Fig. 4b).

Two statistically indistinguishable biotite plateau ages have been obtained for sample TMD 14-9 (Ashton). We obtained an age of 97.4 ± 1.1 Ma (MSWD = 1.07; P = 0.38) on a single biotite grain and 97.8 ± 1.1 Ma (MSWD = 0.8; P = 0.78) on a multi-grain aliquot (Figs. 4c and 4d). These two $^{40}Ar/^{39}Ar$ ages are indistinguishable from the U-Pb age at 96.30 ± 1 Ma obtained by Merle et al. (2006) on titanite and zircon fractions from the same sample. $^{40}Ar/^{39}Ar$ dating of amphibole crystals from sample TMD 21-1 from Seine seamount yielded three indistinguishable plateau ages at 24.4 ± 0.4 Ma (MSWD = 0.23; P = 1.0) and 24.4 ± 0.5 Ma (MSWD = 1.24; P = 0.26) for the single grain measurements (Figs. 4e and 4f) and 24.8 ± 0.3 Ma (MSWD = 1.72; P = 0.13) for the multi-grains aliquot measurements (Fig. 4g). These

ages are slightly older than the previous age at 22.0 ± 0.2 Ma (recalculated using an age of 28.34 Ma for the TCs standard; Renne et al., 1998) obtained on groundmass by Geldmacher et al. (2005). For the two first aliquots, the $^{40}Ar/^{36}Ar$ intercept values on the inverse isochron diagrams are similar to the atmospheric ratio. The third aliquots displays a value higher than the atmospheric ratio and a much greater scatter of the data suggesting that some heterogeneously distributed excess $^{40}Ar^*$ might be present (Fig. 4-5). The third aliquot is therefore not included in the mean age calculation of TMD 21-1 (Table 4).

Discussion

Significance of the new $^{40}Ar/^{39}Ar$ ages

The activity on the northernmost Bikini Bottom seamount estimated at >90 Ma may be related to the Cretaceous phase already pointed out by the previous studies (Geldmacher et al., 2006; Merle et al., 2006) but the poor age data quality prevent us from further speculation. Similar poor data quality for the Torillon seamount suggests a magmatic activity at ≥60 Ma in this locality. The $^{40}Ar/^{39}Ar$ biotite ages obtained from the trachyte TMD14-9 sampled on the Ashton seamount are indistinguishable from the U-Pb age (96.3 ± 1.0 Ma, Merle et al., 2006) yielded by titanite and zircon fractions extracted from the same rock. This implies that the zircon grains extracted from this alkaline lava have a magmatic origin as proposed by Merle et al. (2006) and are not inherited from the continental lithosphere. Nevertheless, this does not exclude the occurrence of the continental lithosphere beneath the seamount since Ashton is located at its very edge (Fig. 1b). Considering that the $^{40}Ar/^{39}Ar$ ages only marginally allow the expected ~1% intercalibration bias with U-Pb ages within errors (Min et al., 2000; Mundil et al., 2006), the data also seem to indicate minimal pre-eruptive magma residence times (e.g.

Simon et al., 2008). Our new ages obtained on the lavas from the Seine seamount (24.4 ± 0.5 Ma) are reliable for sub-million year high-precision geochronology and confirm the occurrence of a magmatic activity during the Late Oligocene.

TMR and surroundings age reliability

Precise and accurate radio-isotopic data play a critical role in obtaining the timing, duration, and rates of magmatic processes occurring on the TMR. The new data documented here confirm a long lasting and geographically extended magmatic activity during the Cretaceous and the early Palaeocene. However, any geodynamical discussion must be based on a reliable age database and must be filtered from statistically and geologically untrustworthy measurements. The calculation of the alteration index (A.I., Baski, 2007) to test the accuracy of the $^{40}Ar/^{39}Ar$ measurements was impossible since the detailed $^{40}Ar/^{39}Ar$ dataset (%^{39}Ar released, $^{40}Ar^*/^{39}Ar_K$, apparent age for each step) of the previously dated samples (Geldmacher et al., 2005, 2006, 2008) were not published.

$^{40}Ar/^{39}Ar$ geochronology performed on whole rock and groundmass may be an interesting alternative when K-rich phenocryst phases are absent (Sharp et al., 1996), providing that whole rock acid etching is performed before measurements. This technique can in some case yield good results (e.g. Pringle et al., 1991). Nevertheless, it becomes increasingly clear that K-Ar and $^{40}Ar/^{39}Ar$ measurement on groundmass displays technical limitations for high-precision and accuracy geochronology (except when rocks are only a couple of m.y. old; e.g., Hofmann et al., 2000; Baksi et al., 2006; Jourdan et al., 2007a). These limitations are:

(1) Untestable freshness of the samples using the Ca/K ratio, because different minerals with different chemical compositions and activation energies will degas their Ar at various temperatures yielding complex Ca/K spectra.

(2) $^{40}Ar/^{36}Ar$ fractionation in the extraction line and sample chamber which is known to yield older apparent ages (McDougall and Harrison, 1999).

(3) Existence of fast neutron activation-induced ^{39}Ar and ^{37}Ar recoil and possible ejection (Turner & Cadogan, 1974) creating significant ^{39}Ar and ^{37}Ar loss at the edge of a grain. In most cases, this will result in apparent older age due to the dominant effect of the ^{39}Ar loss (e.g. Onstott et al., 1995; Paine et al., 2006; Jourdan et al., 2007b) but for samples with high Ca/K and significant atmospheric contamination, the recoil of ^{37}Ar may produce younger apparent ages due to recoil fractionation of Ca-derived ^{37}Ar and ^{36}Ar (e.g., Jourdan et al., 2007b). The recoil phenomenon may also involve a complex re-distribution of the daughter atoms in different lattice sites.

Basaltic groundmass samples are generally enriched in potassium relative to the high Ca/K plagioclase phases, yielding age with better precision compared to mineral separates (due to low Ca interference correction and the larger Ar-ion beam). This is evidenced by our amphibole age (24.4 ± 0.4 Ma) from Seine seamount (Figs. 1 and 4) which is less precise than the earlier matrix age (22.0 ± 0.2 Ma; Geldmacher et al., 2005). However, it has been shown than in most cases for rocks older than a couple of Ma, the accuracy of the age obtained on the groundmass might be questionable (e.g. Hofmann et al., 2000; Jourdan et al., 2007a). Here, we suggest that the age at ~22 Ma of Geldmacher et al. (2005) is ~2 Ma younger due to the occurrence of cryptic alteration phases in the groundmass.

Furthermore, in basaltic rocks, the fine-grained groundmass carries most of the potassium (Mankinen and Dalrymple, 1972) and thus renders the K-Ar and $^{40}Ar/^{39}Ar$ measurements largely dependent on the mobility of potassium during any geological event.

382 This limitation is exacerbated for dredged rocks because they are highly suspected to have
383 undergone severe and pervasive rock-seawater interactions for millions of years leading to a
384 systematic chemical effect on the rock chemistry. This effects are illustrated by the
385 geochemical composition of the TMR samples in which the pervasive seawater-rock
386 interaction led to crystallization of potassium rich secondary phases such as zeolites
387 (erionites, phillipsites), clay-minerals (celadonite-dioctaedric clays mixture) and carbonates
388 in voids and groundmass of the rocks (Fig. 6; Merle, 2006). The crystallization of these
389 alteration phases (brownstone facies, Cann, 1979) implies an overall hydration of the samples
390 and the mobility of the alkaline elements such as potassium (e.g. Honnorez, 1981). The
391 potassium behaviour can be monitored in the TMR samples by a K_2O *vs* LOI diagram in
392 which the LOI values can be used as a proxy for alteration index. For a LOI value higher than
393 4.5%, the K_2O content of the TMR rocks displays a positive co-variation with increasing LOI
394 (Fig. 7). Such kind of co-variation trend has already been documented in submarine samples
395 and interpreted as a potassium accumulation from seawater in the samples (e.g. Honnorez,
396 1981). Therefore, the potassium content of the groundmass of TMR samples might reflect
397 both magmatic composition and seawater interactions. The potassium mobility in basaltic
398 rocks related to seawater interaction might occur even for LOI values lower than 2% (Caroff
399 et al., 1995). As illustrated by the TMR samples, the most careful selection of fresh rock
400 fragments based on optical methods is inadequate since alteration phases are almost inevitably
401 present (see Fig. 6). The effects of pervasive seawater alteration may affect the chemistry of
402 the rocks so deeply that they are unlikely removed by any acid etching compromising
403 groundmass K-Ar and $^{40}Ar/^{39}Ar$ analyses.
404
405 *Filtered age database and standard recalibration*
406

In order to produce a robust age database to support the geodynamical discussion, $^{40}Ar/^{39}Ar$ total fusion measurements as well as K-Ar ages are rejected since there is no mean to check the validity of the age with internal criteria (e.g., age spectrum). Since our new step-heating Ar-Ar amphibole age from Seine is close to the previously published step-heating Ar-Ar matrix age, we consider that the step-heating matrix $^{40}Ar/^{39}Ar$ ages, even if unreliable for high-precision geochronology might have a geological significance and are taken into consideration. We only take into account the $^{40}Ar/^{39}Ar$ plateaus (>70% of ^{39}Ar released) and mini-plateaus (between 50 and 70% of ^{39}Ar released). $^{40}Ar/^{39}Ar$ step-heating measurements having less than 50% of ^{39}Ar are considered as invalid (e.g. Baksi, 1999, McDougall and Harrison, 1999) and are rejected.

U-Pb and $^{40}Ar/^{39}Ar$ age data where tested using the goodness of fit parameters such as the mean squared weighted deviation (MSWD) and probability of fit (P). These parameters were calculated when lacking and are reported in Table 4 along with the filtered database. Interestingly, all the groundmass $^{40}Ar/^{39}Ar$ measurements fit the statistical test, however, as stated before, they still have to be considered with caution. In the following geodynamical discussion, groundmass $^{40}Ar/^{39}Ar$ data will be considered as good estimate, but care must be taken if these data need to be used for very high-precision geochronology. All the $^{40}Ar/^{39}Ar$ data reported in Table 4 are calculated for an age of 28.03 Ma for FCs (Jourdan and Renne, 2007) corresponding to an age of 28.34 Ma for TCs.

Age and duration of magmatic activity on the TMR and surroundings

Considering the available filtered TMR age database, 3 pulses of alkaline magmatism seem to occur from the end of the Early Cretaceous until the Late Paleogene (Fig. 8). The oldest magmatic phase occurred between 103 and 80.5 Ma (magmatic phase 1) in the northern

and the central part of the TMR (Fig. 1). The activity on the northernmost Bikini Bottom seamount estimated at ~90 Ma could be related to this phase. It is also possible that this magmatic phase occurred in the southern part of the TMR since the age of the Lion seamount has been estimated at ~80 Ma (Geldmacher et al., 2006).

A second pulse of magmatism occurred on the TMR during the Late Cretaceous-Early Paleocene (magmatic phase 2) between ~70 and ~60 Ma (Fig. 8). This phase would be localised on the southern part of the TMR and on the Godzilla seamount but could have also taken place on the northern part of the TMR since the magmatic activity on the Torillon seamount has been estimated to be ≥60 Ma (Fig. 1). However, the existence of this phase is based on relatively few data and additional data with a similar age are desirable to constrain the timing and duration of this phase as a significant magmatic event at the TMR scale. Considering the few samples collected, we do not exclude that continuous magmatism could occur from 103 to around 60 Ma with a lack of sampling for the 80-60 Ma period.

The last magmatic phase on the TMR (magmatic phase 3) began around 28 Ma in the southern part of the TMR (Seine-Unicorn area, Figs. 1 and 8). The duration of this magmatic pulse relies upon a number of groundmass $^{40}Ar/^{39}Ar$ analyses and seems to persist until present in the central part (Josephine area, Fig. 1) and southern part of the rise, leading to the construction of the Madeira archipelago.

Considering the magmatic activity that occurred between 88 and 69 Ma (n = 10) on the coast of Portugal (Grange et al., 2007) and at 65-62 Ma (n = 3) on Ormonde seamount (Féraud et al., 1982, 1986; Table 4), magmas were emitted continuously from 103 to 62 Ma in the northern central Atlantic (Fig. 1). An U-Pb age of 77 Ma was obtained on a diorite from Ormonde (Schärer et al., 2000) which is significantly older than the numerous previous $^{40}Ar/^{39}Ar$ ages (Féraud et al., 1982, 1986). This sample was collected on the top of Ormonde seamount among drop-stones of various continental petrographic types (Schärer et al., 2000)

and displays geochemical characteristics (similar REE and multi-element patterns, same initial Hf isotopic composition) and age (within uncertainties) similar to the diorites of the Sines complex documented by Grange et al. (2007). As a consequence, this sample is most likely a drop-stone from the Sines complex, not related to the alkaline activity on Ormonde seamount. Magmatic activity might have occurred around 32 Ma on the Ampere-Coral Patch seamounts. However, this age was obtained on groundmass of a dredged sample (Geldmacher et al., 2000) and would require confirmation by $^{40}Ar/^{39}Ar$ on mineral separates. It emerges from this age compilation that a gap in magmatic activity occurred between around 60 and 32 Ma, at least considering the available dataset.

Refining the geodynamical model of the TMR origin

An OIB-type origin for the TMR

All the studied TMR lavas have unambiguous OIB-type geochemical characteristics. The enriched nature of the magmatism is likely to be inherited from the melting of enriched mantle domains (Geldmacher et al., 2005, 2006, 2008; Merle, 2006). Such a geochemical signature argues for a hot-spot-like nature for the origin of TMR (Geldmacher et al., 2006; Merle et al., 2006). An OIB-type magmatism rules out any accretion-related off-axis magmatic activity (Jagoutz et al., 2007), as this model suggests the shallow melting of asthenosphere-like depleted mantle source. Moreover, the emplacement of the TMR seamounts postdates by at least 20 Ma the activity of the accreting centre in the region.

Considering that the TMR magmatism is volumetrically important (~100 x 10^3 km^3) and comparable to the Canary Archipelago magmatism (150 x 10^3 km^3), it is unlikely that it originates from shallow melting processes, such as edge driven convection or adiabatic partial

melting of magma occurring along transform faults. Furthermore, edge-driven convection would require thick cratonic lithosphere in the vicinity (King and Ritsema, 2000), which has not been evidenced beneath Iberia and north-western Africa.

During the TMR magmatic activity (103 Ma – Present), this part of the Iberian margin and the adjacent oceanic area underwent a wide compression (e.g. Olivet, 1996; Sibuet et al., 2004b). A strong heat source is then required to maintain a melting anomaly over the entire region during more than 100 Ma. In the case of a Hawaiian hot-spot model, an increase of the ages along the seamounts chain is expected. In the TMR case, this simple feature is most probably complicated by the complex motion of the Iberian plate since the Early Cretaceous.

Problems about the previous models proposed for the TMR origin

The lack of a clear space-time correlation over the whole area (although local trends may exist) and the simultaneous magmatic activity observed at several places, such as on Tore and Jo Sister seamounts and on the continent (Ribamar intrusion) at ~ 88 Ma, seem to exclude a simple Hawaiian-type hot spot for the origin of the TMR. A recent study proposes that the TMR would have been built during two phases of magmatism, the oldest one during the Cretaceous later capped by a Miocene-Pleistocene phase (Geldmacher et al., 2006). The first phase would be due to the interaction between the Canary hot-spot and the Mid-Atlantic Ridge (MAR), leading to the construction of an oceanic plateau, together with the J-Anomaly Ridge (JAR, located on the south of the Grand Banks of Newfoundland). The TMR and the JAR would constitute the basement of the second Miocene-Pleistocene magmatic phase induced by the activity of the Madeira hot-spot (Geldmacher et al., 2006). In spite of the advantage of giving an attractive geodynamical interpretation, this model presents some problems. (1) According to this model, the Cretaceous basement would correspond to the

deepest part of the TMR and then all the Miocene-Pleistocene rocks would be dredged from shallower depths. However, the dredging depth can not be used to postulate any stratigraphic relations between Cretaceous and Miocene-Pleistocene rocks. Moreover, Cretaceous rocks were sometimes recovered at shallower depth than Miocene-Pleistocene rocks. For instance, the samples from Jo Sister (86-89 Ma) documented by Merle et al. (2006) were dredged between -2224 and -1960 m while the rocks from the eastern slope of the Josephine seamount (14-16 Ma) were dredged between -3600 and -3000 m. (2) The TMR and the JAR would be formed near the ridge axis around 125-130 Ma. Even if the possibility of an interaction with the MAR has been suspected for the oldest part of the TMR (Sponge Bob seamount, Merle et al., 2006), the magmatic activity exclusively younger than 103 Ma documented on the TMR post-dates the spreading of the Atlantic ridge by at least 22 Ma. Moreover, the age of the emplacement of the JAR is not constrained by any isotopic age data. (3) The main problem of this model concerns the seamounts located on the North of the AGFZ, which are not taken into account in the proposed geodynamical interpretation of Geldmacher et al. (2006). If they are included in the proposed plate reconstruction, these seamounts would be in a position to originate from the Madeira hot-spot and not from the Canary hot-spot as proposed, thus contradicting the interpretation of the isotopic signatures (see Fig. 9 in Geldmacher et al., 2006 and discussion concerning the isotopic data). Therefore, if the magmatism of the northern part of the TMR is taken into account, it is necessary to consider the kinematics of the Iberian plate that would necessarily influence the spatial distribution of the seamounts since they lie on the Iberian plate. (4) At last, this model does not include the magmatic alkaline activity occurring on the Portugual coast between 88 and 69 Ma.

A wide, deep rooted thermal anomaly located beneath the Azores, the Canaries and Madeira (Montelli et al., 2004) that could possibly have fed the TMR has also been proposed

as a possible source of magmas leading to the construction of the TMR (Merle et al., 2006). This model however gives no details concerning the space-time related emission of magmas.

New interpretation of the TMR geodynamics

Considering that three temporally and spatially distinct magmatic phases occurred on the TMR and display heterogeneous isotopic signatures (Geldmacher et al., 2005; 2006; 2008; this study), we suggest that short-lived, small-sized (less than 100 km) magma pulses were emitted from a thermal anomaly located under the TMR-Azores-Madeira-Canary area. These magmatic pulses do not seem to be emitted randomly since two local trends are observed between Sponge Bob and Jo Sister seamounts (103-86 Ma) and between Ribamar and Serra de Monchique on the continent (88-69 Ma; Fig. 1b). The oceanic trend is oriented NE-SW suggesting a north-eastward motion of the Iberian plate. The continental trend is oriented NNW-SSE, suggesting a NNW motion of the Iberian plate. The movement of the Iberian plate since the Late Jurassic has been debated for three decades. However, a recent comprehensive geodynamical reconstruction of the Iberia plate motion and the Pyrenees orogenic formation (Sibuet et al., 2004b) suggests a plate motion toward the NE from 125 to around 83 Ma and toward the NNW from 83 Ma until Present (Fig. 9a). This model reconciles the onland data from the Pyrenees orogen formation and the offshore data from the Iberian margin and the Bay of Biscay. It suggests that part of the Neo-Tethys ocean was located between Iberia and Europe during the Late Jurassic-Early Cretaceous. This geodynamical reconstruction of the Iberian region (Sibuet et al., 2004b) together with our data allow us to propose a geodynamical model that involves an interaction between a thermal anomaly emitting magmatic pulses and the motion of the Iberia plate.

555 Stage 1 – 103 to 88 Ma: the Iberia plate moved in a NE direction due to the subduction
556 of the Neo-Tethys Ocean beneath Europe (Fig. 9a). During this period, the Iberia behaved as a
557 part of the African plate and the plate boundary was located in the Bay of Biscay and the
558 Pyrenees. The emission of a magmatic pulse during this period yields to the formation of the
559 age trend observed from Sponge Bob to Jo Sister (Fig. 9b) corresponding to the magmatic
560 phase 1 on the TMR.

561 Stage 2 – ~88 to 81 Ma: the kinematics of the Iberian plate changed drastically around
562 83 Ma. The spreading of the Bay of Biscay ceased and the subduction of the Neo-Tethys
563 ocean was achieved (Fig. 9a). The motion of the Iberia plate shifted from SW-NE to SSE-
564 NNE leading to little or no movement during this stage. This change would need several
565 million years to be effective, which led to a heat accumulation in the underneath mantle by
566 the blanketing effect of the lithosphere. As a consequence, the thermal anomaly becomes
567 hotter. It induced the emission of several magmatic pulses on distinct locations on the TMR as
568 well as the Portugual coast. This may explain the occurrence of randomly-located magmatism
569 between 88 and 81 Ma which ended the magmatic phase 1 on the TMR (Fig. 9b). It is
570 possible that the lithospheric structures may have drained the ascending magmas.

571 Stage 3 – 80 to 69 Ma: as the continental subduction of Iberia under Europe initiated,
572 the Iberian plate started moving toward the NNW (Fig. 9a). The magmatic pulse already
573 emitted during the previous stage along the Portugal coast produced an age trend from the
574 Ribamar intrusion to the Serra de Monchique complex (Fig. 9b, Grange et al., 2007).

575 Stage 4 – ~68 to 60 Ma: a second period of randomly-located magmatism occurred,
576 corresponding to the magmatic phase 2 on the TMR (Fig. 9b). As for stage 2, this phase could
577 be associated with a period of quiescence in the motion of the Iberia plate, leading again to
578 the accumulation of heat under the lithosphere and emission of several magmatic pulses. Such
579 a motionless phase has not been described in the model proposed by Sibuet et al. (2004b; see

580 Fig. 9a). However, considering the duration of the NNW motion phase in this model (~85 Ma
581 to Present), a brief motionless period may have occurred as identified between 69 and 56 Ma
582 by Roest & Srivastava (1991).

583 Stage 5 – 56 to 33 Ma: during this period, no magmatism is identified either on the
584 continent or in the oceanic domain (Fig. 9b). This period corresponds to the main
585 compression phase of the Pyrenees orogenesis (Olivet, 1996; Sibuet et al., 2004b). During this
586 period, a 90 km-long slab of the oceanic lithosphere of the Bay of Biscay was subducted
587 beneath the northern coast of the Iberian peninsula, along the North Iberian trough (Olivet,
588 1996 and references included). This subduction led to a thrust zone extending from the
589 Pyrenees oceanward to the side of the Galicia bank (e.g. Olivet, 1996; Thinon et al., 2001). It
590 is likely that a wide and strong compression affected both oceanic and continental
591 lithospheres located on the south of the Galicia bank, as evidenced by the northward thrust of
592 the Gorringe bank on the Tagus Abyssal Plain in the Early Tertiary times (Olivet, 1996; Le
593 Gall et al., 1997). This wide compression that affected both oceanic and continental
594 lithospheres may have prevented the ascent of the magmas toward the surface.

595 Stage 6 – ~32 Ma to present: The Pyrenees orogen is built and the plate boundary
596 between the European and African plates is now the AGFZ (Fig. 9a). The Iberian plate
597 consequently behaved as part of the European plate. The convergence between Europe and
598 Africa, which involved an overall compression on the Iberia peninsula, is still ongoing
599 (Jiménez-Munt, 2001). This period is related to another phase of randomly emitted magmatic
600 pulses. This magmatic activity corresponds to the magmatic phase 3 on the TMR. The
601 compression state on Iberia may have prevented the emission of the magma at the surface and
602 may explain the localization of magmatism on the African plate. The very slow motion of the
603 African plate (< 2mm/yr; Stich et al., 2006) may favour heat accumulation under the
604 lithosphere by a shield effect and lead to an increase of magmatic pulse emissions. The

position of the magmatic occurrences close to the branches of the AGFZ (Fig. 9b) suggests that these lithospheric structures may have played a role of conduits to drain the magmas to the surface.

Considering the geochronological, geochemical and isotopic data published on the TMR and the new $^{40}Ar/^{39}Ar$ data presented here, the magmatic phases on the TMR are mirrored by the interaction of a wide thermal anomaly beneath the lithosphere and the Iberia Plate motion driven by orogenic and tectonic activity of the Pyrenees. This model satisfies the geodynamical constraints imposed by the kinematics of the Iberia plate.

A single magmatic province in the Northern central Atlantic?

On the American plate, several seamount groups (Corner seamounts: 80-76 Ma; Newfoundland seamounts: 98 Ma; sills drilled on the ODP leg 210, site 1276: 105-98 Ma and New England seamounts: 103-82 Ma) had magmatic activity contemporaneous with that of the TMR (Fig. 10) and were located at that time less than 1000 km from the TMR. Although most of these ages were obtained by either K-Ar or $^{40}Ar/^{39}Ar$ on groundmass, they suggest that a wide magmatic activity occurred around 105 Ma on the northern central Atlantic. It is not excluded that the Azores Archipelago (from ~85 Ma to Present) and the Canary magmatic province (from 55 Ma and possibly 68 Ma to Present; Geldmacher et al., 2005) were also active at the same time as the TMR (Fig. 10). All these magmatic occurrences have previously been considered as independent magmatic provinces. They are relatively close in space to one another (less than 500 km) and seem to emplace during the same period. Recent geochemical studies have put forward that these provinces may share similar isotopic characteristics and thus, similar mantle source. For instance, the isotopic compositions of Madeira and Canary archipelagos, New England seamounts and some TMR lavas tend to

converge to a restricted composition corresponding to a HIMU-like mantle component (Low Velocity Component: LVC defined by Hoernle et al., 1995; Taras and Hart, 1987; Geldmacher and Hoernle, 2000; Geldmacher et al., 2006). Similar source and coeval period of magmatic activity in the Northern Central Atlantic ocean together with the thermal anomaly imaged by seismic tomography (Montelli et al., 2004) argue for a single magmatic province fed by a wide thermal anomaly as previously proposed for the SW Portugal-Canary-Madeira magmatism (Hoernle et al., 1995; Lustrino and Wilson, 2007).

However, an isotopic heterogeneity is observed between the different provinces but also within a given province, e.g., strong isotopic heterogeneity on São Miguel Island in the Azores (Widom et al., 1997); EMI signature for Godzilla but HIMU for Josephine on the TMR (Geldmacher et al., 2006, 2008); clear EMII component in the ODP leg 210 sills (Hart and Blusztajn, 2006). A hypothesis to reconcile these data is to invoke a wide mantle plume/thermal anomaly which produced scattered magmatic pulses over a very large area yet constituting a single large volcanic province.

Conclusions

Our new $^{40}Ar/^{39}Ar$ measurements of plagioclase, amphibole and biotite separates from the Bikini Bottom, Torillon, Ashton and Seine seamounts give new constraints on the construction of the TMR. The filtered database argues for three magmatic phases on the TMR (103-80 Ma, ~68 Ma and from ~28 Ma until Present). Considering the magmatism that occurred on the Ampere-Coral Patch seamounts, Ormonde seamount and on the Portugal coast, the magmatic activity was continuous from 103 until ~60 Ma and from ~32 Ma until Present. Based on the space and time distribution of the magmatism on the TMR and surroundings, we suggest that the TMR magmatism resulted from interaction between the

complex motion of the Iberian plate due to the Pyrenees formation and a wide thermal anomaly located beneath the Canary-Madeira area. This thermal anomaly produced short-lived, small-scale (> 100km) magmatic pulses which created seamount alignments during the phases of motion of the Iberian plate between 103 and 80 Ma and between 80 and 70 Ma. Instead, during the periods of quiescence of the Iberian plate, the shield effect of the lithosphere (continental and/or oceanic) would involve an accumulation of heat in the mantle leading to an increase of magma emissions. These periods correspond to randomly spatial occurrence of magmatism between 88 and 81 Ma, 67 and 60 Ma and from 31 Ma until Present. During the main compression phase associated with the Pyrenees formation, between 56 and 33 Ma, no magmatism occurred. The overall compression that affected the Iberian plate would prevent magma emission on the surface.

The TMR magmatism could be related to the same geodynamic process that led to the genesis of several magmatic provinces on the northern central Atlantic such as Newfoundland, Corner and New England seamounts, Azores and Canary Archipelagos which emplaced during the same period. All these magmatic occurrences could be the surface expressions of the thermal anomaly now located beneath the Canary-Azores area.

Acknowledgements

We thank the captain and the crew of the R/V *Atalante*. For thin sections and technical assistance we thank E. Boeuf, B. De Quillac and H. Loyen. M. Bohn is thanked for assistance during electron-microprobe analyses. J. Cotten is acknowledged for providing ICP-AES analyses. Constructive comments by Dr. Kelley, Dr. Ukstins-Peate helped to improve the manuscript. We also thank Dr. Sherlock as handling editor.

680 **Appendices**

681

682 **References**

683

684 Baksi, A.K. 1999. Reevaluation of plate motion models based on hotspot tracks in the
685 Atlantic and Indian Oceans. *Journal of Geology*, **107**, 13-26.

686 Baksi, A.K. 2007. A quantitative tool for detecting alteration in undisturbed rocks and
687 minerals—I: Water, chemical weathering, and atmospheric argon. Special Paper 430:
688 Plates, Plumes and Planetary Processes: Vol. 430, 285-303.

689 Bernard-Griffiths, J., Gruau, G., Cornen, G., Azambre, B. & Macé, J., 1997. Continental
690 lithospheric contribution to alkaline magmatism: isotopic (Nd, Sr, Pb) and geochemical
691 (REE) evidence from Serra de Monchique and Mount Ormonde Complexes. *Journal of.*
692 *Petrology*, **38**, 115-132.

693 Cann, J.R., 1979. Metamorphism of oceanic crust. *In*: Talwani M. & Hayes D.E. (eds) *Deep*
694 *drilling results in the Atlantic ocean: ocean crust*. America Geophysical Union
695 Geodynamic Service, 230-238.

696 Carignan, J., Hild, P., Mevelle, G., Morel, J. & Yeghicheyan, D., 2001. Routine analyses of
697 trace element in geological samples using flow injection and low pressure on-line liquid
698 chromatography coupled to ICP-MS: a study of geochemical reference materials BR,
699 DR-N, UB-N, AN-G and GH. *Geostandards Newsletters*, **25**, 187-198.

700 Caroff, M., Bellon H., Chauris L., Carron J.-P., Chevrier S., Gardinier A., Cotten J., Le Moan
701 Y. & Neidhart Y. 1995. Magmatisme fissural triasico-liasique dans l'ouest du Massif
702 Armoricain (France): pétrologie, géochimie, âge, et modalités de la mise en place.
703 *Canadian Journal of Earth Sciences*, **32**, 1921-1936.

704 Cornen, G. 1982. Petrology of the alkaline volcanism of Gorringe Bank (southwest Portugal).
705 *Marine Geology*, **47**, 101-130.
706 Cotten, J., Le Dez, A., Bau M., Caroff M., Maury R.C., Dulsky P., Fourcade S., Bohn M. &
707 Brousse R. 1995. Origin of anomalous rare-earth elements and yttrium enrichments in
708 subaerially exposed basalts: evidence from french Polynesia. *Chemical Geology*, **119**,
709 115-138.
710 Dalrymple, G.B. & Duffield W.A. 1988. High precision $^{40}Ar/^{39}Ar$ dating of Oligocene tephra
711 from the Mogollon-Datil volcanic field using a continuous laser system. *Geophysical*
712 *Research Letters*, **15**, 463-466.
713 Duncan, R. A. 1984. Age progressive volcanism in the New England Seamounts and the
714 opening of the central Atlantic Ocean. *Journal of Geophysical Research*, **89**, 9980-
715 9990.
716 Féraud, G., Gastaud, J., Auzende, J.M., Olivet, J.L. & Cornen G. 1982. $^{40}Ar/^{39}Ar$ ages for the
717 alkaline volcanism and basement of Gorringe Bank, North Atlantic Ocean. *Earth*
718 *Planetary Sciences Letters*, **57**, 211-226.
719 Féraud, G., York, D., Mével, C., Cornen, G. & Auzende J-M. 1986. Additionnal $^{40}Ar/^{39}Ar$
720 dating of the basement and alkaline volcanism of the Gorringe Bank (Atlantic Ocean).
721 *Earth and Planetary Sciences Letters*, **79**, 255-269.
722 Duffield, W. A. & Dalrymple G. B. 1990. Taylor Creek rhyolite of New Mexico, a rapidly
723 emplaced field of domes and flows. *Bulletin of Volcanology*, **52**, 475-487.
724 Geldmacher, J., Van der Bogaard, P., Hoernle, K. & Schmincke H.-U. 2000. The $^{40}Ar/^{39}Ar$
725 age dating of the Madeira Archipelago and hotspot track (eastern North Atlantic).
726 *Geochemistry Geophysics Geosystems*, 1, doi:10.1029/1999GC000018.

727 Geldmacher, J. & Hoernle K. 2000. The 72 Ma geochemical evolution of the Madeira hotspot
728 (eastern North Atlantic): recycling of Paleozoic (≤ 500 Ma) oceanic lithosphere. *Earth*
729 *and Planetary Sciences Letters*, **183**, 73-92.
730 Geldmacher, J., Hoernle, K., Van der Bogaard, P., Zankl G. & Garbe-Schönberg D. 2001.
731 Earlier history of the ≥70Ma old Canary hotspot based on the temporal and geochemical
732 evolution of the Selvagen Archipelago and neighboring seamounts in the eastern North
733 Atlantic. *Journal of Volcanology and Geothermal Research*, **111**, 55-87.
734 Geldmacher, J., Hoernle, K., Van den Bogaard, P., Duggen S. & Werner R. 2005. New
735 $^{40}Ar/^{39}Ar$ age geochemical seamounts Canary and Madeira volcanic provinces: Support
736 for the mantle plume hypothesis. *Earth and Planetary Sciences Letters,* **237**, 85-101.
737 Geldmacher, J., Hoernle K., Klügel A., Van den Bogaard P., Wombacher F. & Berning B.
738 2006. Origin and geochemical evolution of the Tore-Madeira Rise (eastern North
739 Atlantic). *Journal of Geophysal Research*, B09206, doi:10.1029/2005JB003931.
740 Geldmacher, J., Hoernle, K., Klügel, A., Van der Bogaard P. & Bindeman I. 2008.
741 Geochemistry of a new enriched mantle type locality in the northern hemisphere:
742 Implications for the origin of the EM-I source. *Earth and Planetary Sciences Letters,*
743 **265**, 167-182.
744 Gente, P., Dyment, J., Maia, M. & Goslin, J. 2003. Interaction between the Mid-Atlantic
745 Ridge and the Azores hot-spot during the last 85 Myr: emplacement and rifting of the
746 hot-spot-derived plateaus. *Geochemistry Geophysics Geosystems*, **4**,
747 doi:10.1029/2003GC0052.
748 Girardeau, J., Cornen, G., Beslier, M.-O., Le Gall, B., Monnier, C., Agrinier, P., Dubuisson,
749 G., Pinheiro, L., Ribeiro, A. & Whitechurch, H. 1998. Extensional tectonics in the
750 Gorringe Bank rocks, Eastern Atlantic ocean: evidence of an oceanic ultra-slow
751 mantellic accreting centre. *Terra Nova*, 10, 330-336.

752 Govindaraju, K. & Mevelle G. 1987. Fully automated dissolution and separation methods for
753 inductively coupled plasma atomic emission spectrometry rock analysis. Application to
754 the determination of rare earth elements. *Journal of Analytical Atomic Spectrometry,* **2**,
755 615-621.
756 Grange, M., Schärer, U., Cornen, G. & Girardeau, J. 2007. Time-space migration of melting
757 within the East Atlantic plume and magmatism of Portugal: U-Pb ages and Pb-Sr-Hf
758 isotopes. Goldschmidt Conference Annual Meeting, Cologne, Germany.
759 Hart, S.R. & Blusztajn, J. 2006. Age and geochemistry of the mafic sills, ODP site 1276,
760 Newfoundland margin, *Chemical Geology*, **235**, 222-237.
761 Hofmann, C., Féraud, G. & Courtillot, V. 2000. $^{40}Ar/^{39}Ar$ dating of mineral separates and
762 whole rocks from the Western Ghats lava pile: further constraints on duration and age
763 of the Deccan traps. *Earth and Planetary. Sciences Letters*, **180**, 13-27.
764 Honnorez, J. 1981. The aging of the oceanic crust at low temperature. *In*: Emiliani, C. (ed)
765 *The sea: the oceanic lithosphere*, Wiley, New York, 525-587.
766 Hoernle, K., Zhang, Y.S., Graham, D., 1995. Seismic and geochemical evidence for large-
767 scale mantle upwelling beneath the eastern Atlantic and western and central Europe.
768 *Nature*, **374**, 34-39.
769 Jagoutz, O., Müntener, O., Manatschal, G., Rubatto, D., Péron-Pinvidic, G., Turrin, B.D. &
770 Villa, I.M. 2007. The rift-to-drift transition in the North Atlantic: A stuttering start of
771 the MORB machine?, *Geology*, **35**, 1087-1090.
772 Jiménez-Munt, I., Fernandez, M., Torne, M. & Bird, P. 2001.The transition from linear to
773 diffuse plate boundary in the Azores-Gibraltar region: results from a thin-sheet model.
774 *Earth and Planetary Sciences Letter,* **192**, 175-189.
775 Jourdan, F. & Renne, P.R. 2007. Age calibration of the Fish Canyon sanidine $^{40}Ar/^{39}Ar$ dating
776 standard using primary K-Ar standards. *Geochimica Cosmochimica Acta*, **71**, 387-402.

777 Jourdan, F., Féraud, G., Bertrand, H., Watkeys, M.K. & Renne P.R., 2007a. Distinct brief
778 major events in the Karoo large igneous province clarified by new $^{40}Ar/^{39}Ar$ ages on the
779 Lesotho basalts. *Lithos,* **98**, 195-209.
780 Jourdan, F., Matzel, J.P. & Renne, P.R. 2007b. ^{39}Ar and ^{37}Ar recoil loss during neutron
781 irradiation of sanidine and plagioclase, *Geochimica Cosmochimica Acta,* **71**, 2791-
782 2808.
783 King, S.D. & Ritsema, J. 2000. African hotspot volcanism smallscale, convection in the upper
784 mantle beneath cratons. *Science*, **290**, 1137-1140.
785 Le Gall, B., Piqué, A., Réhault, J.P., Specht, M. & Malod, J. 1997. Structure et mise en place
786 d'une ride océanique dans un contexte de limite de plaque convergente. *Comptes Rendus*
787 *Academie Sciences Paris*, **325**, 853-860.
788 Lustrino, M. & Wilson M. 2007. The circum-Mediterranean anorogenic Cenozoic igneous
789 province. *Earth-Science Reviews*, **81**, 1-65.
790 McDougall, I. & Harrison, T.M. 1999. *Geochronology and Thermochronology by the*
791 *$^{40}Ar/^{39}Ar$ Method*. Oxford University Press, Oxford.
792 Merle, R. 2006. Age and origin of Tore-Madeira Rise: Beginning of Atlantic Ocean spreading
793 or hotspot track. Petrology, Geochemistry, U-Pb Geochronology and Pb-Sr-Hf isotopes,
794 PhD thesis, University of Nantes.
795 Merle, R., Schärer, U., Girardeau, J. & Cornen, G. 2006. Cretaceous seamounts along the
796 ocean-continent of Iberian margin: U-Pb ages and Sr-Pb-Hf isotopes. *Geochimica*
797 *Cosmochimica Acta*, **70**, 4950-4976.
798 Min, K., Mundil, R., Renne, P.R. & Ludwig, K.R. 2000. A test for systematic errors in
799 $^{40}Ar/^{39}Ar$ geochronology through comparison with U–Pb analysis of a 1.1 Ga rhyolite.
800 *Geochimica Cosmochimica Acta*, **64**, 73-98.

Montelli, R., Nolet, G., Dahlen, F. A., Masters, G., Engdahl E. R. & Hung, S.H. 2004. Finite-frequency tomography reveals a variety of plume in the mantle. *Nature*, **303**, 338-343.

Mundil, R., Renne, P.R., Min K.K. & Ludwig, K.R. 2006. Resolvable miscalibration of the $^{40}Ar/^{39}Ar$ geochronometer. *Eos Trans. AGU*, **87**, Fall Meet. Suppl., Abstract V21A-0543.

Olivet, J.-L. 1996. La cinématique de la plaque Ibérique, *Bulletin Centres Recherches Exploration-Production Elf Aquitaine*, **20**, 131-195.

Onstott, T.C., Miller, M.L., Ewing, R.C. & Walsh, D. 1995. Recoil refinements: implications for the $^{40}Ar/^{39}Ar$ dating technique. *Geochimica Cosmochimica Acta*, **59**, 1821-1834.

Paine, J.H., Nomade, S. & Renne, P.R. 2006. Quantification of ^{39}Ar recoil ejection from GA1550 biotite during neutron irradiation as a function of grain dimensions. *Geochimica Cosmochimica Acta*, **70**, 1507-1517.

Peirce, C. & Barton, P.J. 1991. Crustal structure of the Tore-Madeira Rise, Eastern North Atlantic-results of a DOBS wide-angle and normal incidence seismic experiment in the Josephine Seamount region. *Geophysical Journal International*, **106**, 357-378.

Pringle, M.S., Staudigel, H. & Gee, J. 1991. Jasper Seamount: Seven million years of volcanism. *Geology*, **19**, 364-368.

Renne, P.R., Swisher, C.C., Deino, A.L., Karner, D.B., Owens, T.L., & DePaolo, D.J. 1998. Intercalibration of standards, absolute ages and uncertainties in $^{40}Ar/^{39}Ar$ dating. *Chemical Geology*, **145**, 117-152.

Roest, W.R. & Srivastava, S.P. 1991. Kinematics of the plate boundaries between Eurasia, Iberia and Africa in the North Atlantic from the Late Cretaceous to the present. *Geology*, **19**, 613-616.

824 Schärer, U., Girardeau, J., Cornen, G. & Boillot, G. 2000. 138-121 Ma asthenospheric
825 magmatism prior to continental break-up in the North Atlantic and geodynamic
826 implications. *Earth and Planetary Sciences Letters*, **181**, 555-572.
827 Sibuet, J.-C., Monti, S., Loubrieu, B., Mazé, J.-P. & Srivastava S. 2004a. Carte bathymétrique
828 de l'Atlantique nord-est et du golfe de Gascogne : implications géodynamiques. *Bulletin de*
829 *la Societe Géologique de France*, **175**, 429-442.
830 Sibuet, J.-C., Srivastava S. & Spakman W. 2004b. Pyrenean orogeny and plate kinematics.
831 *Journal of Geophysical Research*, **108**, B08104.
832 Simon, J.I., Renne, P.R. & Mundil, R. 2008. Implications of pre-eruptive magmatic histories
833 of zircons for U–Pb geochronology of silicic extrusions. *Earth and Planetary Science*
834 *Letters*, **266**, 182-194.
835 Sircombe, K.N. 2004. AgeDisplay: An EXCEL workbook to evaluate and display univariate
836 geochronological data using binned frequency histograms and probability density
837 distributions. *Computers and Geosciences*, **30**, 21-31.
838 Steiger, R.H. & Jäger E. 1977. Subcommission on geochronology: convention on the use of
839 decay constants in geo- and cosmochronology. *Earth and Planetary Sciences Letters*,
840 **36**, 359-362.
841 Stich, D., Serpelloni, E., Mancilla, F. de L. & Morales, J. 2006. Kinematics of the Iberia-
842 Maghreb plate contact from seismic, moment tensors and GPS observations.
843 *Tectonophysics*, **426**, 295-317.
844 Sullivan, K.D., & C.E. Keen 1977. Newfoundland seamounts: Petrology and geochemistry,
845 *Geological Association of Canada Special Paper*, **16**, 461-476.
846 Sun, S.S. & McDonough, W.F. 1989. Chemical and isotopic systematics of oceanic basalts:
847 implication for mantle composition and processes. *In*: Saunders, A.D. & Norry, M.J.

(eds) *Magmatism in the ocean basins*. Geological Society, London, Special Publications, **42**, 313-345.

Taras, B.D. & Hart, S.R. 1987. Geochemical evolution of the New England seamount chain: isotopic and trace element constraints. *Chemical Geology*, **64**, 35-54.

Thinon, I., Fidalgo-González, L., Réhault, J.-P. & Olivet J.-L. 2001. Déformations pyrénéennes dans le golfe de Gascogne. *Comptes Rendus Academie Sciences Paris*, **332**, 561-568.

Turner, G. & Cadogan, P. 1974. Possible effects of ^{39}Ar recoil in ^{40}Ar/^{39}Ar dating. *Proceeding 5th Lunar Planetary Science Conference*, 1601-1615.

Van der Linden W.J.M. 1979. The Atlantic margin of Iberia and Morocco, a reinterpretation. *Tectonophysics*, **59**, 185-199.

Wendt, I., Kreuzer, H., Muller, P., Von Rad, U. & Raschka, H. 1976. K-Ar age of basalts from Great Meteor and Josephine seamount (eastern North Atlantic). *Deep-Sea Research*, **23**, 849-862.

Widom, E., Carlson, R.W., Gill, J.B. & Schmincke, H.-U. 1997. Th-Sr-Nd-Pb isotope and trace elements evidence for the origin of the São Miguel, Azores, enriched mantle source. *Chemical Geology,* **140***,* 49-68.

Figures captions

Figure 1: (a) Bathymetric map of the East northern central Atlantic (From Sibuet et al., 2004a). TAP: Tagus abyssal plain. (b) Bathymetric map of the study region distinguishing the main structural units. Solid lines represent faults, and dashed lines inferred faults. AGFZ: Azores-Gibraltar Fracture Zone. Triangles indicate seamounts where dating has been performed. Ages of Ormonde, Monchique, Madeira, Porto Santo, Desertas Islands, Ampere, Josephine, Unicorn

and Seine from Wendt et., 1976: Féraud et al., 1982; 1986; Bernard-Griffiths et al., 1997; Geldmacher et al., 2000; 2005, 2006; 2008; Merle et al., 2006). The geochronological data from this study are indicated in bold. Location of the J anomaly after Olivet (1996).

Figure 2: Primitive mantle-normalized trace elements patterns. Normalization values from Sun and McDonough (1989). Average N-MORB pattern from Sun and McDonough (1989). Pattern of previously studied samples from Seine seamount after Geldmacher et al. (2005).

Figure 3: Zr/Yb vsTh/Nb plot for the data-points of the TMR samples. Fields of Canary Archipelago and Madeira Archipelago basalts and Atlantic N-MORBs from Georoc and PetDB databases. Field of previously studied TMR samples from Geldmacher et al. (2005; 2006; 2008).

Figure 4: Plagioclase, biotite and amphibole $^{40}Ar/^{39}Ar$ apparent age and related Ca/K ratio spectra of the plagioclase separates versus the cumulative percentage of ^{39}Ar released. Errors on plateau (>70% ^{39}Ar released) and mini-plateau (50-70% ^{39}Ar released) ages are quoted at 2σ and do not include systematic errors (i.e. uncertainties on the age of the monitor and on the decay constant). MSWD and probability are indicated. Ages in bold represent the most reliable ages for each sample.

Figure 5: Inverse correlation isochron plot of $^{36}Ar/^{40}Ar$ vs. $^{39}Ar/^{40}Ar$ for two step-heated samples. MSWD and probability, and $^{40}Ar/^{36}Ar$ intercept are indicated. Excluded steps are indicated in gray.

Figure 6: Photographs of thin sections of basic and less evolved lavas dredged on the TMR. The vesicles are filled by clay minerals, zeolites and carbonates. The groundmass display also overall oxidation due to seawater percolation.

Figure 7: Variation of potassium content as function of seawater alteration expressed as LOI (Loss on Ignition). The discrepancy observed for LOI higher than 4.5 % is related to potassium mobility.

Figure 8: Age frequency histogram (error bars not included) and probability density distribution diagram (PDD; error bars included in the curve calculation; PDD increment: 0.5 Ma) for the TMR lavas.

Figure 9: Geodynamical model for the space-time repartition of magmatism on TMR and surroundings. (a): Locations of the Iberian Plate since 125 Ma relative to Europe considered to be fixed (adapted from Sibuet et al., 2004b). The light gray domains are areas in extension and dark gray domains are areas under compression. The double lines in the Bay of Biscay at 83 Ma indicate the proto-ridge. J, A33 and A 34 are magnetic anomalies. The black arrows indicate the direction of convergence and the white arrows, the direction of extension. EU: Europe plate; IB: Iberian plate; NA: North America plate. Pyr suture: Pyrenees suture. NGFZ: Newfoundland Gibraltar fracture zone. (b) Interpretation of magmatic activity on the TMR and surroundings as different stages corresponding to the phases of the Iberian plate motion and Pyrenees orogenesis. Gray arrows indicate the magmatic trends.

Figure 10: Location of the different magmatic occurrences in the Northern Central Atlantic Ocean close to the TMR area at the time of its activity. Estimation of the volcanic activity of Azores from Gente et al. (2003); age of the ODP 210 sills from Hart and Blusztajn (2006);

922 age of the New England seamounts from Duncan (1984); Newfoundland seamounts from
923 Sullivan and Keen (1977). Range of the magmatic activity on the Canaries from Geldmacher
924 et al. (2001).
925
926 Tables
927
928 Table 1: Sampling sites and dredging operations parameters.
929 Table 2: Major and trace elements analyses of TMR.
930 Table 3: $^{40}Ar/^{39}Ar$ results.
931 Table 4: Filtered geochronological data from TMR and surroundings.

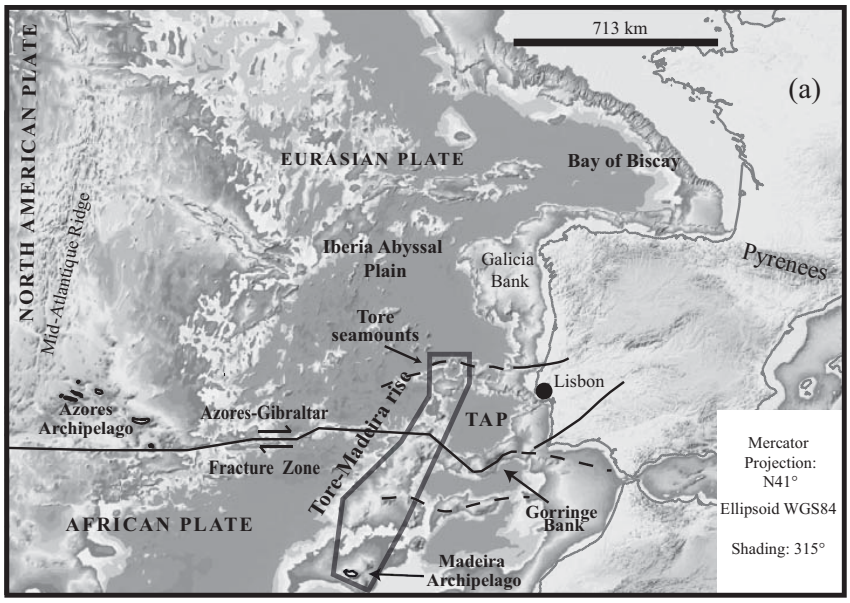
713 km
(a)
NORTH AMERICAN PLATE
Mid-Atlantique Ridge
EURASIAN PLATE
Bay of Biscay
Iberia Abyssal Plain
Galicia Bank
Pyrenees
Tore seamounts
Lisbon
Azores Archipelago
Azores-Gibraltar Fracture Zone
Tore-Madeira rise
TAP
AFRICAN PLATE
Gorringe Bank
Madeira Archipelago
Mercator Projection: N41°
Ellipsoid WGS84
Shading: 315°

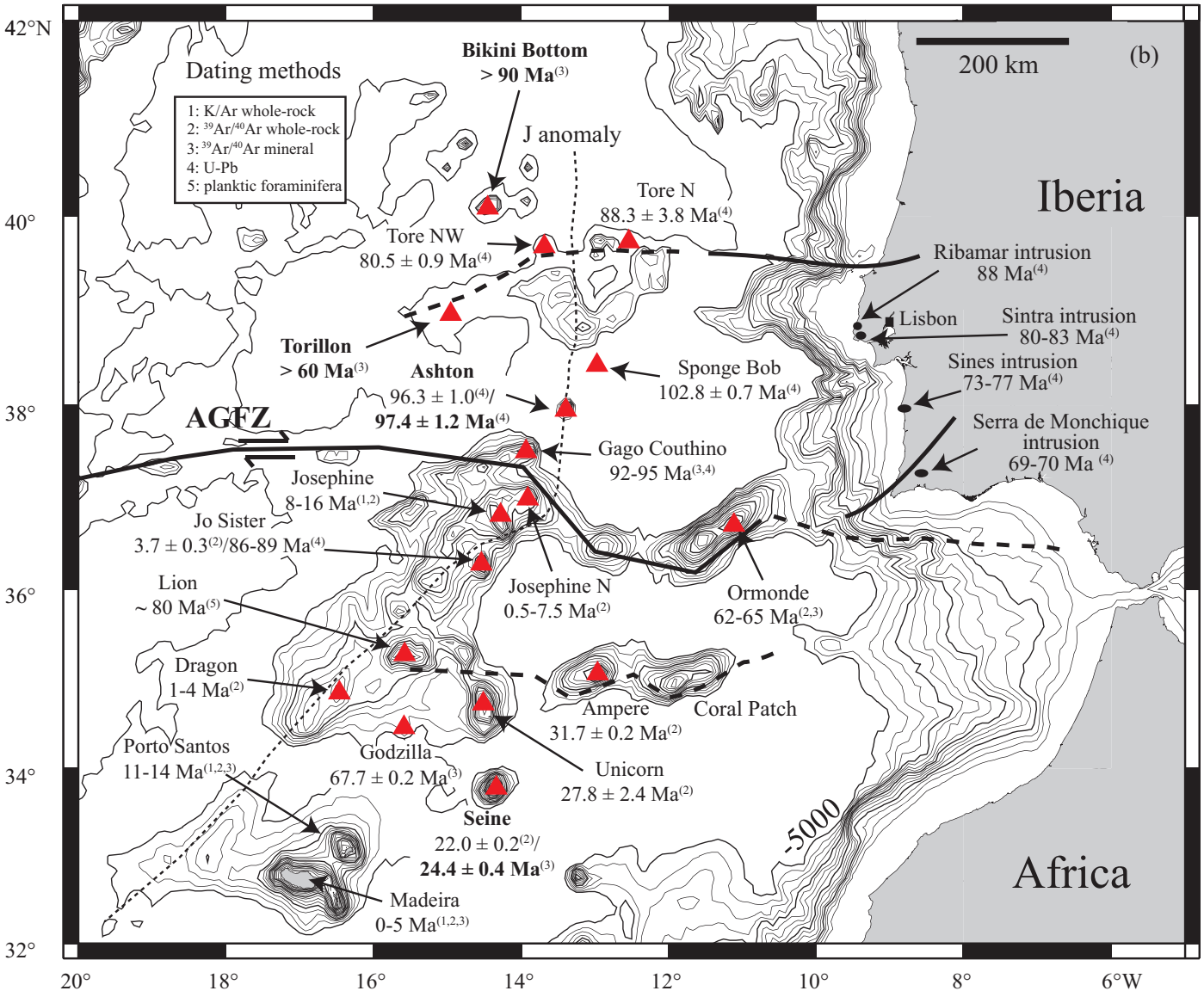
42°N
40°
38°
36°
34°
32°
20°
18°
16°
14°
12°
10°
8°
6°W
200 km
(b)
Dating methods
1: K/Ar whole-rock
2: 39Ar/40Ar whole-rock
3: 39Ar/40Ar mineral
4: U-Pb
5: planktic foraminifera
Bikini Bottom
> 90 Ma(3)
J anomaly
Tore N
88.3 ± 3.8 Ma(4)
Tore NW
80.5 ± 0.9 Ma(4)
Iberia
Ribamar intrusion
88 Ma(4)
Lisbon
Sintra intrusion
80-83 Ma(4)
Torillon
> 60 Ma(3)
Ashton
96.3 ± 1.0(4)/
97.4 ± 1.2 Ma(4)
Sponge Bob
102.8 ± 0.7 Ma(4)
Sines intrusion
73-77 Ma(4)
AGFZ
Serra de Monchique intrusion
69-70 Ma (4)
Gago Couthino
92-95 Ma(3,4)
Josephine
8-16 Ma(1,2)
Jo Sister
3.7 ± 0.3(2)/86-89 Ma(4)
Lion
~ 80 Ma(5)
Josephine N
0.5-7.5 Ma(2)
Ormonde
62-65 Ma(2,3)
Dragon
1-4 Ma(2)
Ampere
31.7 ± 0.2 Ma(2)
Coral Patch
Porto Santos
11-14 Ma(1,2,3)
Godzilla
67.7 ± 0.2 Ma(3)
Unicorn
27.8 ± 2.4 Ma(2)
Seine
22.0 ± 0.2(2)/
24.4 ± 0.4 Ma(3)
-5000
Africa
Madeira
0-5 Ma(1,2,3)

Figure 1

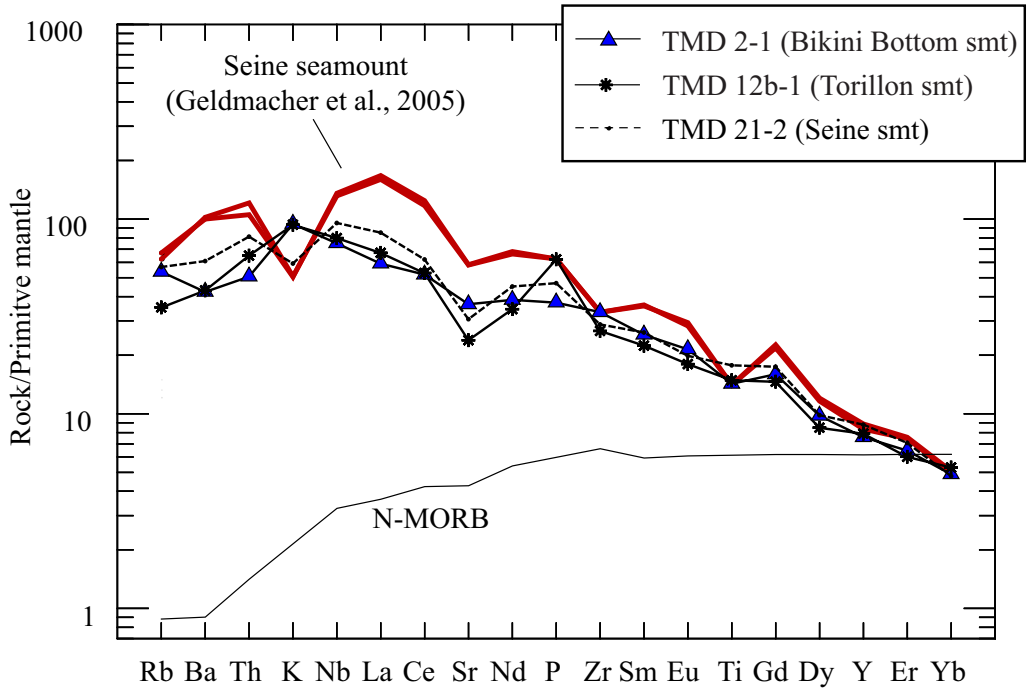
1000
100
10
1
Rock/Primitve mantle
Seine seamount
(Geldmacher et al., 2005)
N-MORB
TMD 2-1 (Bikini Bottom smt)
TMD 12b-1 (Torillon smt)
TMD 21-2 (Seine smt)
Rb Ba Th K Nb La Ce Sr Nd P Zr Sm Eu Ti Gd Dy Y Er Yb

Figure 2

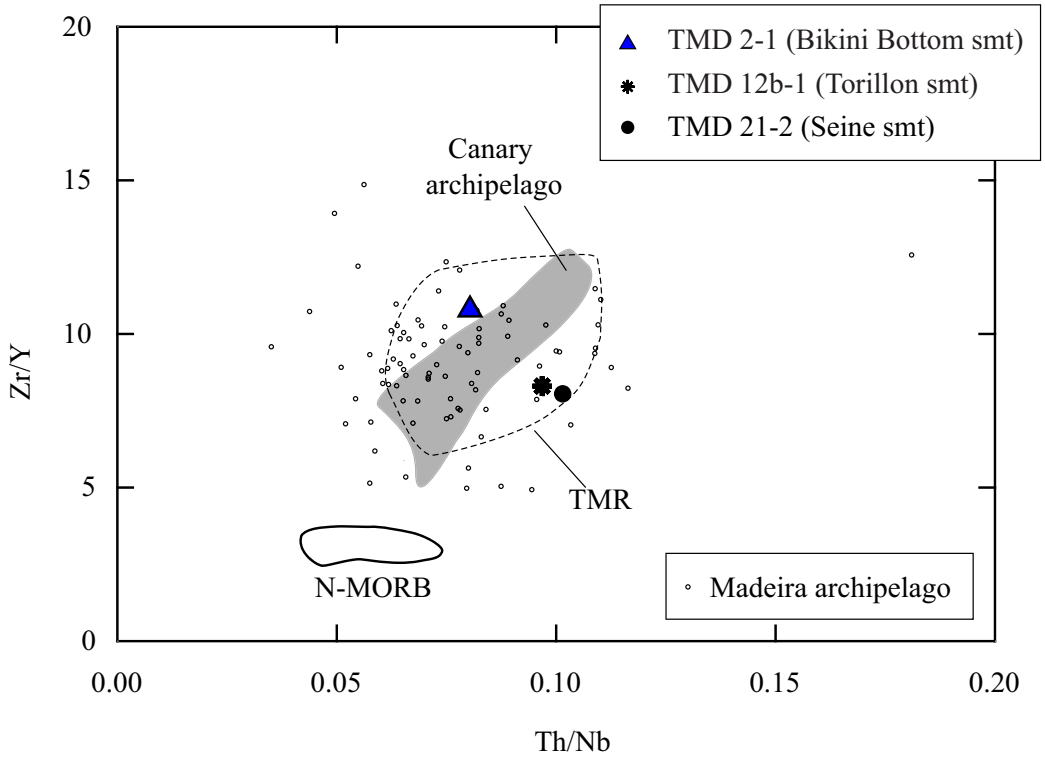
TMD 2-1 (Bikini Bottom smt)
TMD 12b-1 (Torillon smt)
TMD 21-2 (Seine smt)
Canary archipelago
TMR
N-MORB
Madeira archipelago
Zr/Y
Th/Nb
0
5
10
15
20
0.00
0.05
0.10
0.15
0.20

Figure 3

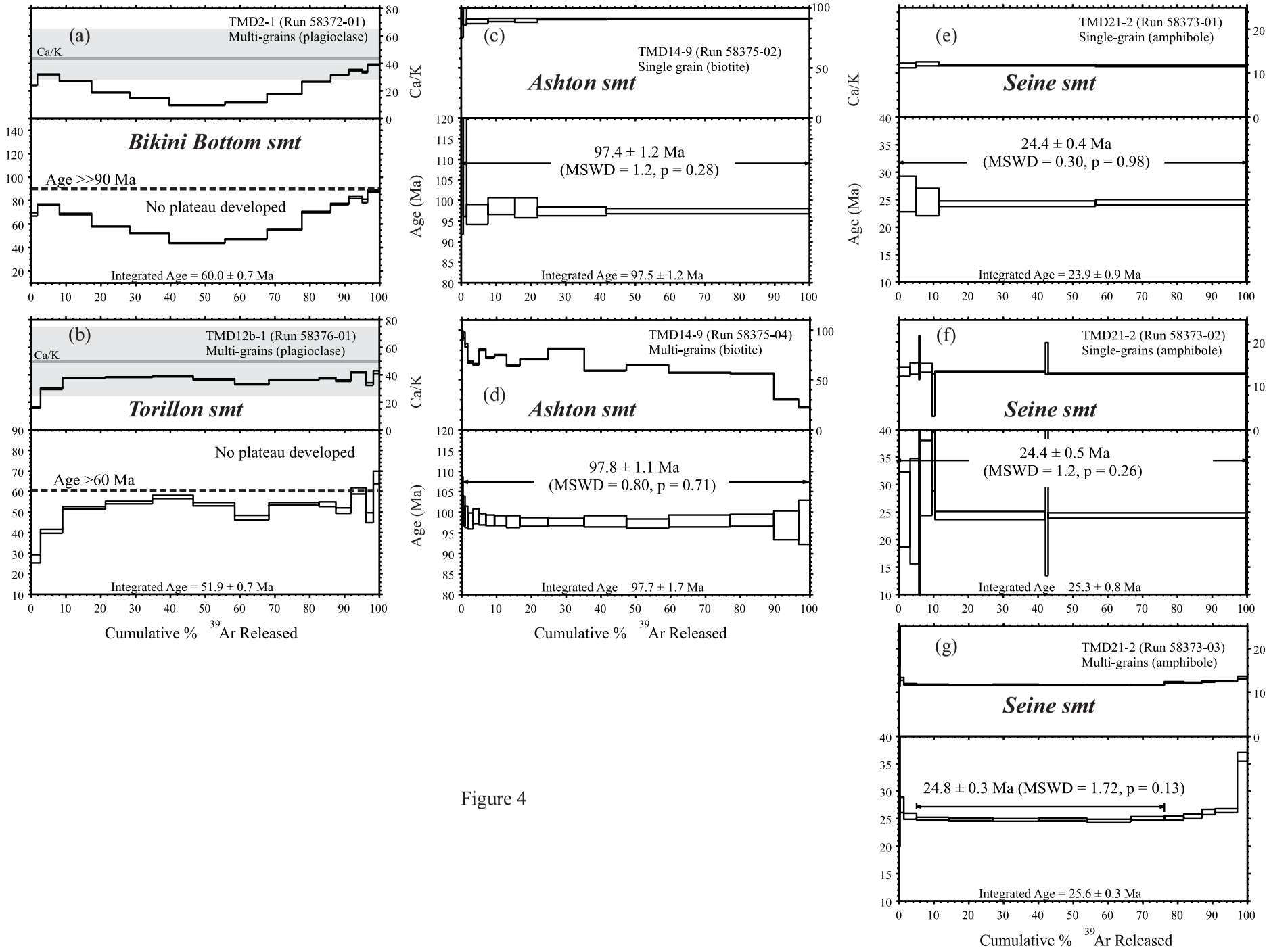
(a)
TMD2-1 (Run 58372-01)
Multi-grains (plagioclase)
Ca/K
Bikini Bottom smt
Age >>90 Ma
No plateau developed
Integrated Age = 60.0 ± 0.7 Ma
(b)
TMD12b-1 (Run 58376-01)
Multi-grains (plagioclase)
Ca/K
Torillon smt
No plateau developed
Age >60 Ma
Integrated Age = 51.9 ± 0.7 Ma
(c)
TMD14-9 (Run 58375-02)
Single grain (biotite)
Ashton smt
97.4 ± 1.2 Ma
(MSWD = 1.2, p = 0.28)
Integrated Age = 97.5 ± 1.2 Ma
(d)
TMD14-9 (Run 58375-04)
Multi-grains (biotite)
Ashton smt
97.8 ± 1.1 Ma
(MSWD = 0.80, p = 0.71)
Integrated Age = 97.7 ± 1.7 Ma
(e)
TMD21-2 (Run 58373-01)
Single-grain (amphibole)
Seine smt
24.4 ± 0.4 Ma
(MSWD = 0.30, p = 0.98)
Integrated Age = 23.9 ± 0.9 Ma
(f)
TMD21-2 (Run 58373-02)
Single-grains (amphibole)
Seine smt
24.4 ± 0.5 Ma
(MSWD = 1.2, p = 0.26)
Integrated Age = 25.3 ± 0.8 Ma
(g)
TMD21-2 (Run 58373-03)
Multi-grains (amphibole)
Seine smt
24.8 ± 0.3 Ma (MSWD = 1.72, p = 0.13)
Integrated Age = 25.6 ± 0.3 Ma
Age (Ma)
Ca/K
Cumulative % 39Ar Released

Figure 4

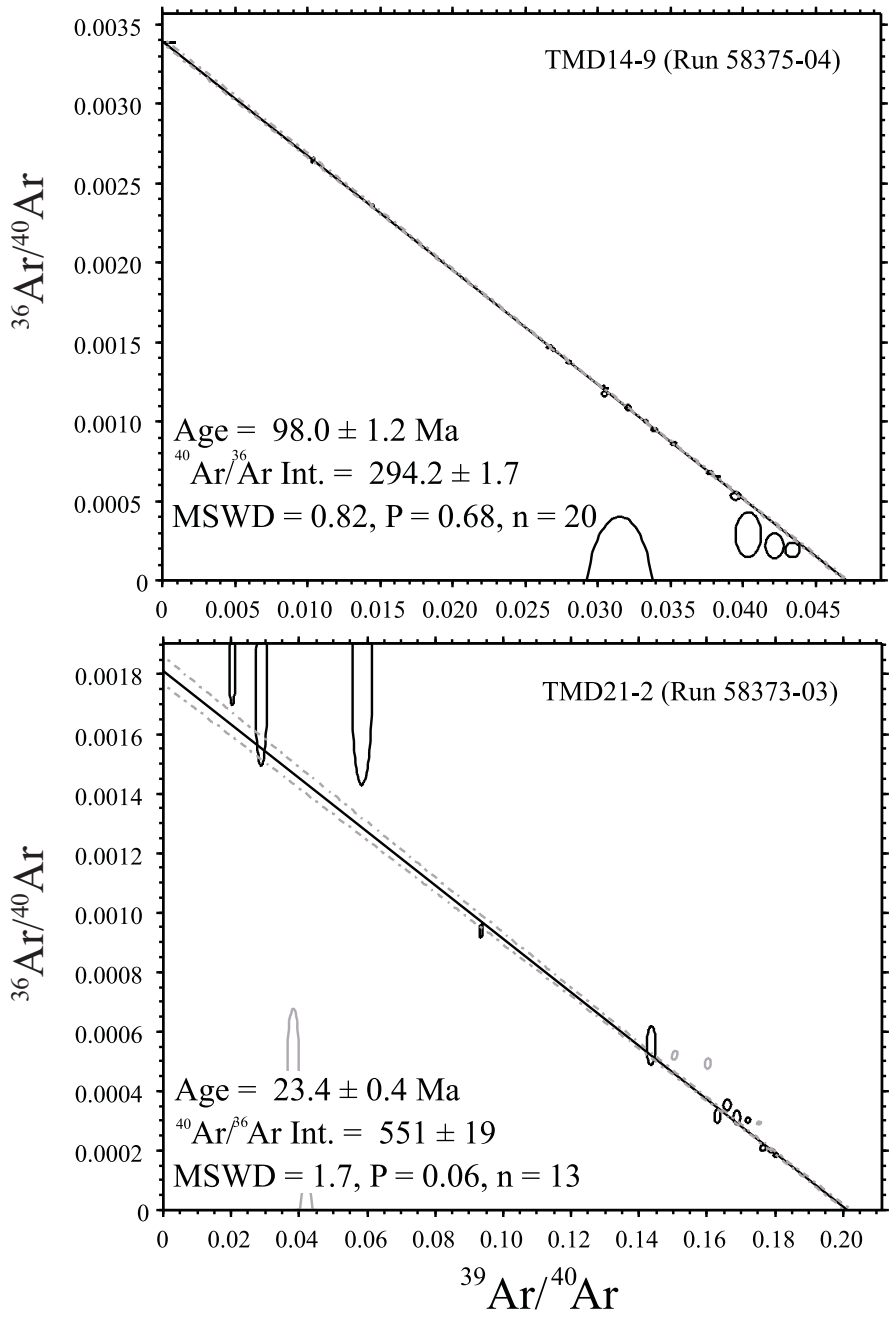
TMD14-9 (Run 58375-04)
Age = 98.0 ± 1.2 Ma
40Ar/36Ar Int. = 294.2 ± 1.7
MSWD = 0.82, P = 0.68, n = 20
TMD21-2 (Run 58373-03)
Age = 23.4 ± 0.4 Ma
40Ar/36Ar Int. = 551 ± 19
MSWD = 1.7, P = 0.06, n = 13
36Ar/40Ar
39Ar/40Ar

Figure 5

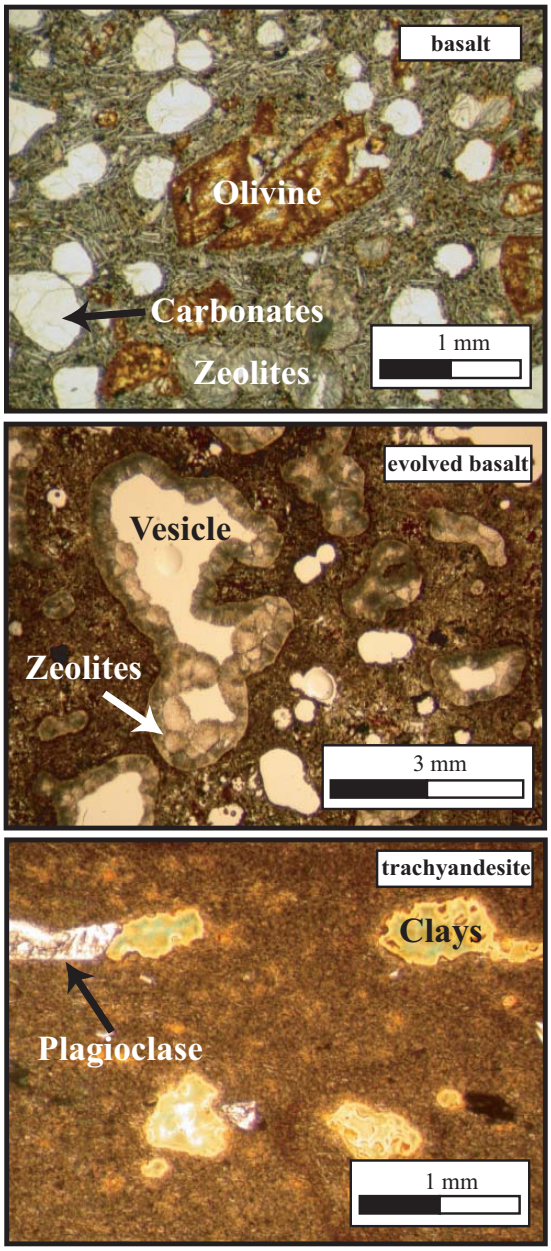
basalt
Olivine
Carbonates
Zeolites
1 mm
evolved basalt
Vesicle
Zeolites
3 mm
trachyandesite
Clays
Plagioclase
1 mm

Figure 6

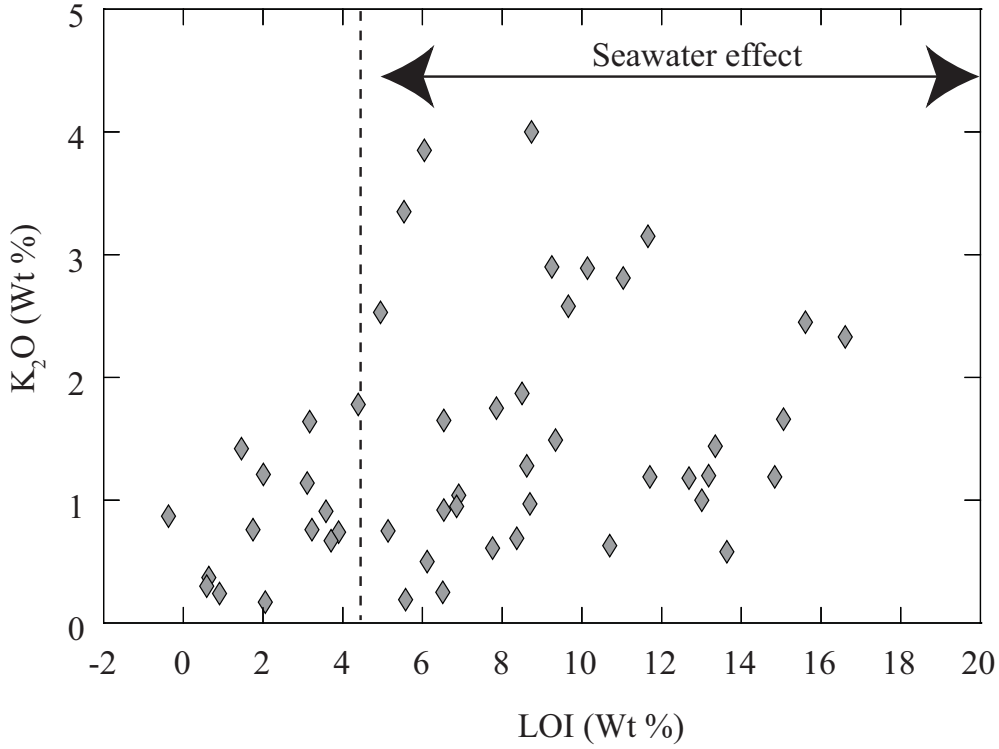

Figure 7

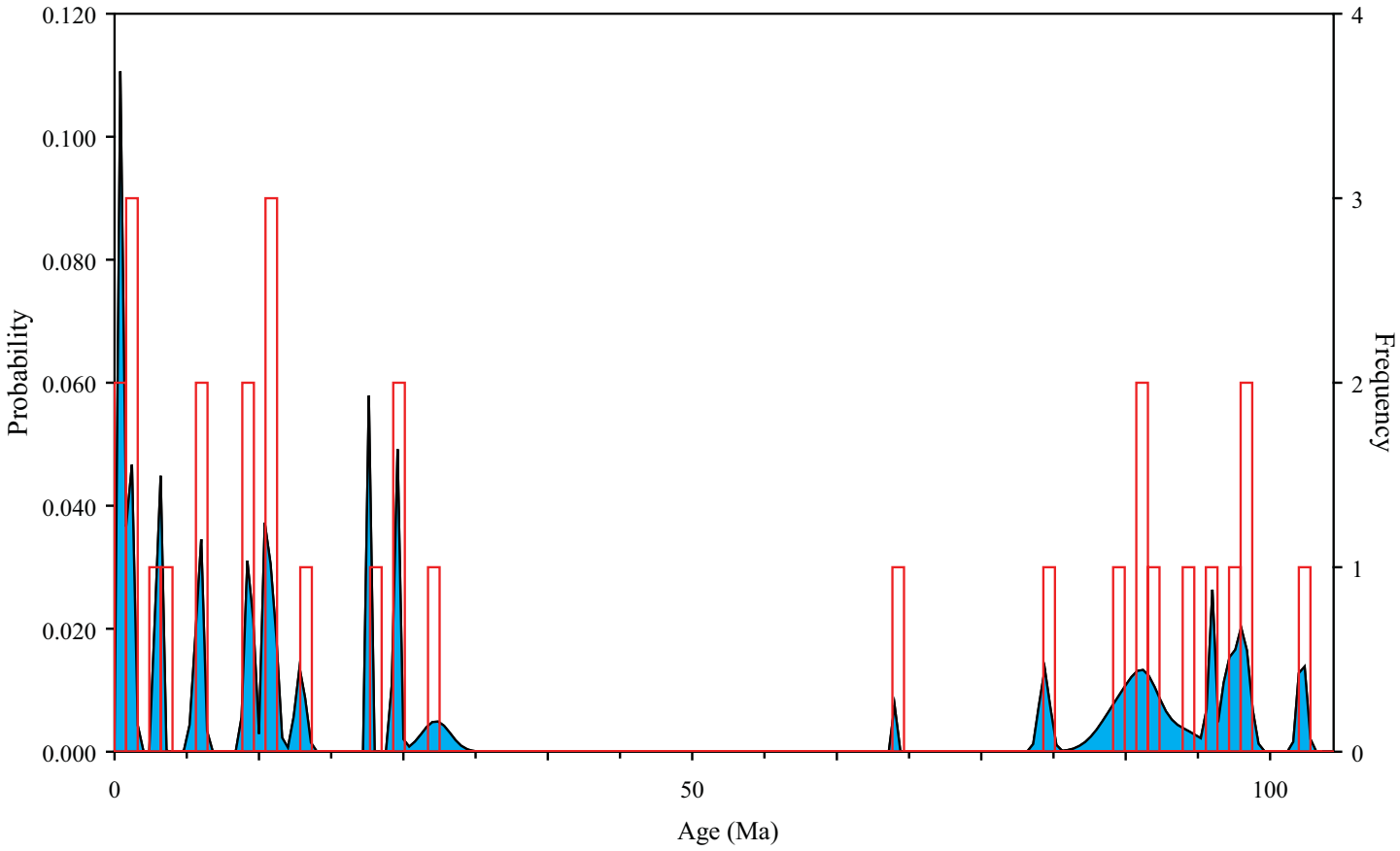
0.120
0.100
0.080
0.060
0.040
0.020
0.000
Probability
4
3
2
1
0
Frequency
0
50
100
Age (Ma)

Figure 8

(a)

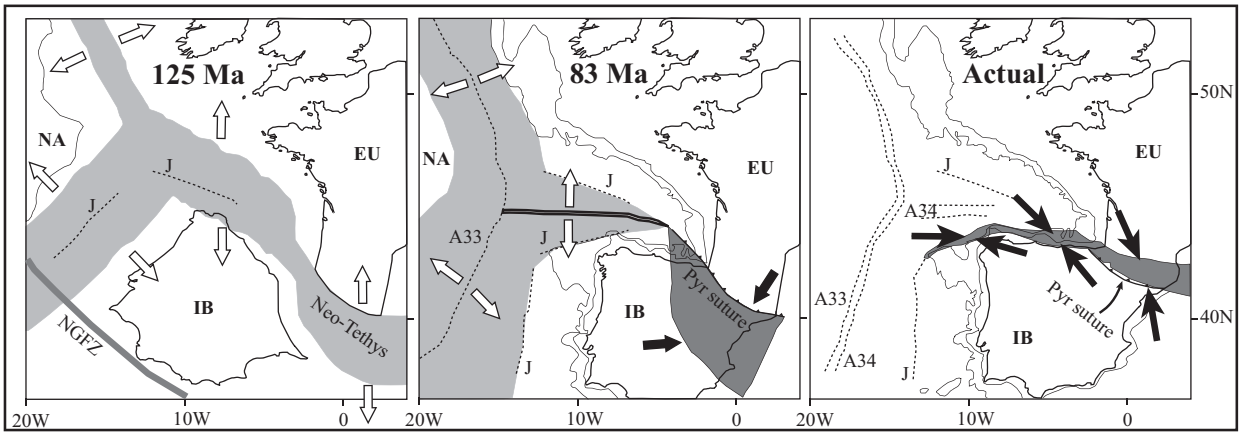
125 Ma
NA
EU
J
J
IB
NGFZ
Neo-Tethys
83 Ma
NA
EU
J
A33
J
IB
Pyr suture
J
Actual
50N
EU
J
A34
A33
Pyr suture
40N
IB
A34
J
20W
10W
0
20W
10W
0
20W
10W
0

(b)

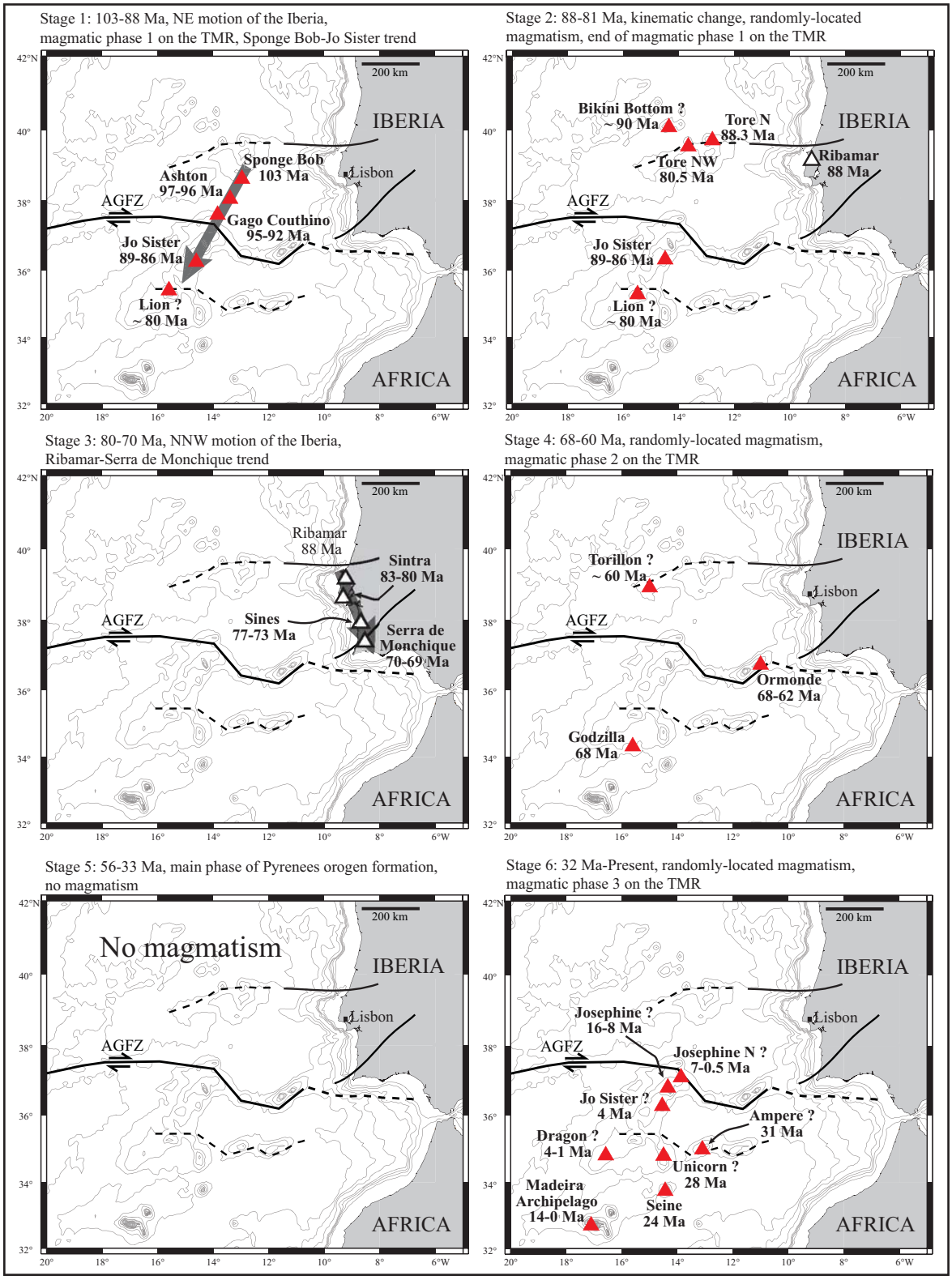
Stage 1: 103-88 Ma, NE motion of the Iberia, magmatic phase 1 on the TMR, Sponge Bob-Jo Sister trend
Stage 2: 88-81 Ma, kinematic change, randomly-located magmatism, end of magmatic phase 1 on the TMR
Stage 3: 80-70 Ma, NNW motion of the Iberia, Ribamar-Serra de Monchique trend
Stage 4: 68-60 Ma, randomly-located magmatism, magmatic phase 2 on the TMR
Stage 5: 56-33 Ma, main phase of Pyrenees orogen formation, no magmatism
Stage 6: 32 Ma-Present, randomly-located magmatism, magmatic phase 3 on the TMR
200 km
IBERIA
AFRICA
AGFZ
Lisbon
Sponge Bob 103 Ma
Ashton 97-96 Ma
Gago Couthino 95-92 Ma
Jo Sister 89-86 Ma
Lion ? ~ 80 Ma
Bikini Bottom ? ~ 90 Ma
Tore N 88.3 Ma
Tore NW 80.5 Ma
Ribamar 88 Ma
Ribamar 88 Ma
Sintra 83-80 Ma
Sines 77-73 Ma
Serra de Monchique 70-69 Ma
Torillon ? ~ 60 Ma
Ormonde 68-62 Ma
Godzilla 68 Ma
No magmatism
Josephine ? 16-8 Ma
Josephine N ? 7-0.5 Ma
Jo Sister ? 4 Ma
Ampere ? 31 Ma
Dragon ? 4-1 Ma
Unicorn ? 28 Ma
Madeira Archipelago 14-0 Ma
Seine 24 Ma

FIGURE 9

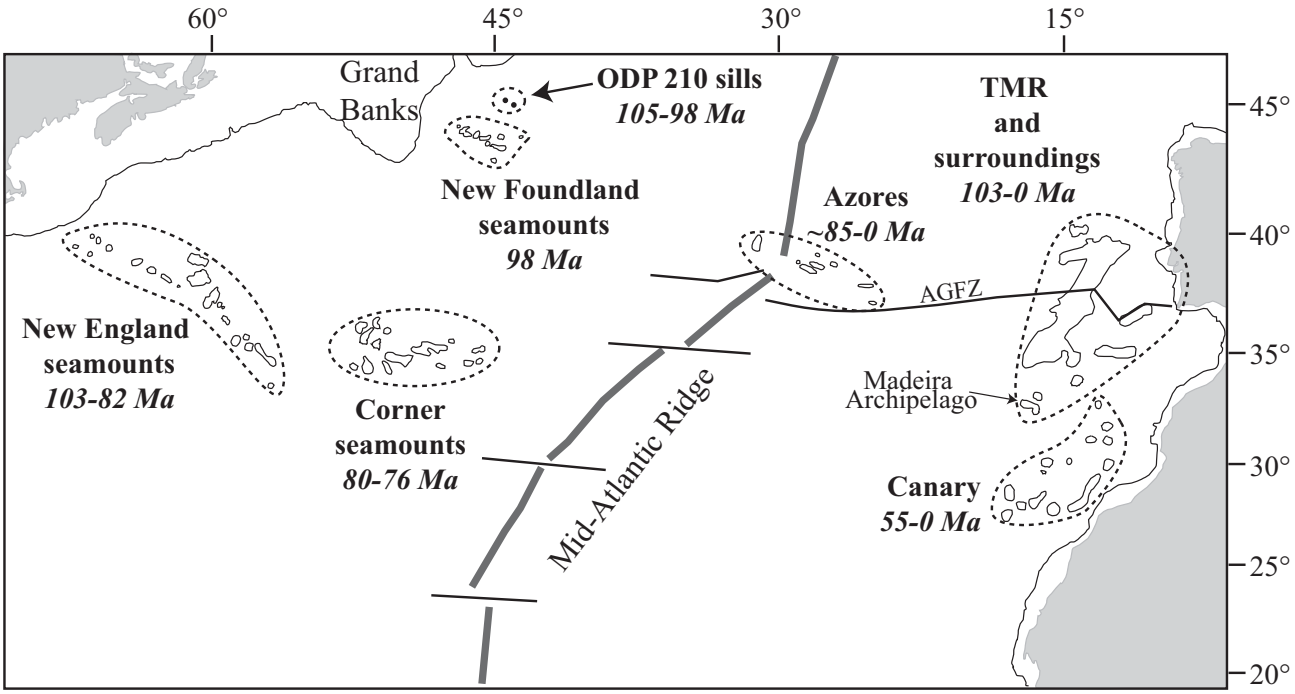
60°
45°
30°
15°
45°
40°
35°
30°
25°
20°
Grand Banks
ODP 210 sills
105-98 Ma
New Foundland seamounts
98 Ma
TMR and surroundings
103-0 Ma
Azores
~85-0 Ma
AGFZ
New England seamounts
103-82 Ma
Corner seamounts
80-76 Ma
Mid-Atlantic Ridge
Madeira Archipelago
Canary
55-0 Ma

Figure 10

Table 1: Sampling sites and dredging operations parameters

Seamount	dredge	Beginning		End		Depth (m)		Distance covered (m)	Height covered (m)
		Lat. (N)	Long. (W)	Lat. (N)	Long. (W)	max	min		
Bikini Bottom	TMD 2	40°03.74'	14°24.50'	40°07.90'	13°39.31'	3514	2234	4074	1280
Torillon	TMD 12b	39°10.63'	15°12.81'	39°11.75'	15°10.51'	3884	3126	2960	758
Ashton	TMD 14	38°01.29'	13°23.71'	38°01.54'	13°22.66'	2803	2395	3900	408
Seine	TMD 21	33°50.83'	14°15.71'	33°51.18'	14°17.22'	1975	1677	1020	298

Table 2: Major and trace elements analyses of TMR

Samples	**TMD2-1**	**TMD 12b-1**	**TMD21-2**
Petrographic type	Basaltic trachy-and	basalt	basanite
(%Wt)			
SiO_2	48.50	40.22	41.10
TiO_2	3.09	3.22	3.84
Al_2O_3	19.20	18.21	13.50
Fe2O3*	10.86	13.38	14.10
MnO	0.20	0.16	0.15
MgO	0.93	1.29	5.75
CaO	6.40	5.58	11.25
NaO	3.79	2.66	2.62
K_2O	2.84	2.81	1.78
P_2O_5	0.81	1.35	1.02
LOI	3.03	11.04	4.39
total	99.65	99.92	99.50
(ppm)			
Rb	34.0	22.3	36.0
Sr	770	503	645
Ba	295	300	425
Sc	15.8	-	26.0
V	220.0	276	368.0
Cr	17.0	93.8	272.0
Co	17.00	33.4	34.50
Ni	9.5	66	112.0
Y	34.5	35.9	40.0
Zr	372	298	322
Nb	53.5	56.9	68.0
La	40.5	46	58.5
Ce	92.0	93.6	110.0
Nd	52.0	46.6	61.0
Sm	11.3	9.92	11.6
Eu	3.60	3.02	3.33
Gd	9.50	8.7	10.40
Dy	7.20	6.24	7.25
Er	3.10	2.88	3.40
Yb	2.41	2.61	2.36
Th	4.30	5.51	6.90

Major and trace elements of samples TMD 2-1 and TMD21-2 were obtained by ICP-AES at Brest (Université de Bretagne Occidentale) following the method described in Cotten et al. (1995). Relative standard deviations are < 2% for major elements, Rb and Sr, and < 5% for other trace elements. Analyses of sample TMD12b-1 were performed at Nancy (SARM, CRPG-CNRS). Major elements were obtained by ICP-AES following the method described in Govindaraju and Mevelle (1987) and trace elements by ICP-MS following the method in Carignan et al. (2001). Analytical precision is at 1-5% for major elements, except for MnO, MgO, Ca_2O and P_2O_5 (10%). For trace elements, analytical precision is in the range 5-10% for abundances > 50 ppm, 5-15% between 50 and 10 ppm, 5-20% between 10 and 1 ppm and 5-25% for abundances < 1 ppm. Fe_2O_3*: total iron expressed as Fe_2O_3. LOI: Loss on ignition. BE-N, AC-E, PM-S and WS-E materials were used as standards.

Table 3: $^{40}Ar/^{39}Ar$ results

General characteristics				Plateau characteristics					Isochron characteristics				
Sample N°	Mineral	Lab N°	Integrated age (Ma, ±2σ)	Plateau age (Ma, ±2σ)	Total ^{39}Ar released (%)	MSWD	P	Mean age* (Ma, ±2σ)	Isochron age (Ma, ±2σ)	n	$^{40}Ar/^{36}Ar$ intercept (±1σ)	MSWD	P
TMD14-9	Biotite	58375-02	97.5 ± 1.2	**97.4 ± 1**	100%	1.2	0.28	**97.7 ± 1.2**	-	-	-	-	-
		58375-04	97.7 ± 1.7	**97.8 ± 1.1**	100%	0.80	0.71		98.0 ± 1.2	20	294.2 ± 1.7	0.82	0.68
TM12b-1	Plagioclase	58376-01	51.9 ± 0.7	-	-	-	-	-	-	-	-	-	-
TMD2-1	Plagioclase	58372-01	60.0 ± 0.7	-	-	-	-	-	-	-	-	-	-
TMD21-2	Amphibole	58373-01	23.9 ± 0.9	**24.4 ± 0.4**	100%	0.3	0.98	**24.4 ± 0.4**	24.4 ± 0.4	16	292 ± 3	0.35	0.99
		58373-02	25.3 ± 0.8	**24.4 ± 0.5**	100%	1.2	0.26		-	-	-	-	-
		58373-03	25.6 ± 0.3	24.8 ± 0.3	71%	1.7	0.13	(excess ^{40}Ar*)?	23.4 ± 0.4	13	551 ± 19	1.7	0.06

Summary table indicating integrated, plateau/mini-plateau and isochron ages for the Tswaing impact glass samples. A (*) indicates mini-plateau ages. MSWD for plateau and isochron, percentage of ^{39}Ar degassed used in the plateau calculation, number of analysis included in the isochron, and $^{40}Ar/^{36}Ar$ intercept are indicated. Plateau age calculated using trapped $^{40}Ar/^{36}Ar$ is indicated. Analytical uncertainties on the ages are quoted at 2 sigma (2σ) confidence levels and at 1σ for the $^{40}Ar/^{36}Ar$ intercept. Bold data indicate the accepted age for a given sample. Italic data indicate rejected analyses.

Table 3: Merle et al.

Table 4: Filtred geochronological data from TMR and surroundings

Reference	Sample name	Location	Phase analyzed	Age (Ma)	Errors (2σ) Ma	MSWD	P
This study	TMD2-1	Bikini Bottom	plag	~ 90			
Merle et al., 2006	TMD10c-1	Tore N	titanite	**88.30**	**3.30**	0.34	0.89
Merle et al., 2006	TMD10c-2	Tore N	titanite	**88.30**	**3.80**	1.01	0.39
Merle et al., 2006	TMD3b-2	Tore NW	titanite+zrc	**80.48**	**0.90**	0.86	0.54
This study	TMD 12b-1	Torillon	plag	~ 60			
Merle et al., 2006	TMD4-3	Sponge Bob	titanite+zrc	**102.77**	**0.71**	0.38	0.91
Merle et al., 2006	TMD14-9	Ashton	titanite+zrc	**96.30**	**1.00**	0.60	0.81
This study	TMD14-9	Ashton	biot	**97.40**	**1.20**	1.20	0.28
This study	TMD14-9	Ashton	biot	**97.80**	**1.10**	0.80	0.71
Merle et al., 2006	TMD15-5	Gago Coutinho	titanite	**92.30**	**3.70**	0.25	0.91
Geldmacher et al., 2006	403 DR-5	Gago Coutinho	hbl	**94.90**	**0.44**	2.00	0.05
Geldmacher et al., 2006	399 DR-1	Josephine N (Pico Pia)	mtrx	0.53	0.45	0.60	0.83
Geldmacher et al., 2006	406 DR-7	Josephine N (Toblerone Ridge)	gls	1.42	0.61	0.70	0.74
Geldmacher et al., 2006	406 DR-7	Josephine N (Toblerone Ridge)	mtrx	0.47	0.13	1.50	0.07
Geldmacher et al., 2006	407 DR-4	Josephine N (Pico Julia)	mtrx	7.09	0.72	0.70	0.74
Geldmacher et al., 2006	407 DR-4	Josephine N (Pico Julia)	mtrx	7.50	0.47	0.60	0.80
Geldmacher et al., 2006	408 DR-2	Josephine	mtrx	16.08	0.87	1.00	0.45
Geldmacher et al., 2006	408 DR-2	Josephine	mtrx	13.83	0.65	1.40	0.14
Geldmacher et al., 2006	409 DR-1	Josephine	mtrx	11.75	0.73	1.30	0.22
Geldmacher et al., 2006	409 DR-1	Josephine	mtrx	11.59	0.65	0.50	0.89
Geldmacher et al., 2006	410 DR-4	Josephine	mtrx	13.35	0.63	0.70	0.78
Geldmacher et al., 2006	410 DR-4	Josephine	mtrx	13.14	0.30	1.60	0.07
Merle et al., 2006	TMD16-1	Jo Sister	titanite	**86.50**	**3.40**	0.13	0.97
Merle et al., 2006	TMD16-2	Jo Sister	titanite	**89.30**	**2.30**	0.76	0.64
Geldmacher et al., 2006	412 DR-2	Jo Sister	mtrx	3.67	0.32	1.70	0.07
Geldmacher et al., 2006	429 DR-1	Dragon	mtrx	1.45	0.43	0.90	0.57
Geldmacher et al., 2006	429 DR-1	Dragon	mtrx	1.14	0.20	0.60	0.73
Geldmacher et al., 2006	431 DR-1	Dragon	mtrx	4.00	0.30	1.30	0.19
Geldmacher et al., 2007	428 DR-1	Godzilla	biot	**67.68**	**0.17**	2.10	0.05
Geldmacher et al., 2005	423 DR-1	Unicorn	mtrx	27.81	2.44	0.70	0.73
Geldmacher et al., 2005	426 DR-1	Seine	mtrx	22.03	0.20	1.20	0.29
This study	TMD21-1	Seine	plag	**24.40**	**0.40**	0.30	0.98
This study	TMD21-1	Seine	plag	**24.40**	**0.50**	1.20	0.26
Geldmacher et al., 2000	DS-797-1	Ampere	mtrx	31.67	0.20	1.33	0.19
Féraud et al., 1982	DR-06-03	Ormonde	biot	**64.30**	1.10	0.65	0.74
Féraud et al., 1982	DR-06-18	Ormonde	mtrx	61.60	**2.40**	0.26	0.91
Féraud et al., 1986	CY14-2	Ormonde	biot	**65.07**	**0.65**	1.30	0.25

The age results reliable for sub-million year high-precision geochronolgy are reported in bold.

Zrc: zircon, biot: biotite, hbl: hornblende, gls: glass, mtx: matrix, plag: plagioclase

Table A1: Geochronological database from TMR and surroundings.

Reference	Sample name	Location	rock type	technique	Phase dated	Age (Ma)	Errors (2σ)	Standard type and age (Ma)
Merle et al., 2006	TMD10c-1	Tore N	trachy-andesite	U-Pb (ID)	titanite	88.30	3.30	-
Merle et al., 2006	TMD10c-2	Tore N	trachy-andesite	U-Pb (ID)	titanite	88.20	3.90	-
Merle et al., 2006	TMD3b-2	Tore NW	trachyte	U-Pb (ID)	titanite+zrc	80.50	0.90	-
Merle et al., 2006	TMD4-3	Sponge Bob	trachyte	U-Pb (ID)	titanite+zrc	102.80	0.70	-
Merle et al., 2006	TMD4-8	Sponge Bob	trachyte	U-Pb (ID)	titanite+zrc	104.40	1.40	-
Merle et al., 2006	TMD14-9	Ashton	trachyte	U-Pb (ID)	titanite+zrc	96.30	1.00	-
Merle et al., 2006	TMD15-5	Gago Coutinho/Teresa	trachyte	U-Pb (ID)	titanite	92.30	3.80	-
Geldmacher et al., 2006	403 DR-5	Gago Coutinho/Teresa	trachyte	$^{40}Ar/^{39}Ar$ (StH)	hbl	94.50	0.43	TCs =27.92
Geldmacher et al., 2006	403 DR-1	Gago Coutinho/Teresa	trachyte	$^{40}Ar/^{39}Ar$ (TF)	hbl	92.50	0.40	TCs =27.92
Geldmacher et al., 2006	399 DR-1	Josephine N (Pico Pia)	basalt	$^{40}Ar/^{39}Ar$ (StH)	mtrx	0.52	0.44	TCs =27.92
Geldmacher et al., 2006	406 DR-7	Josephine N (Toblerone Ridge)	basalt	$^{40}Ar/^{39}Ar$ (StH)	gls	1.40	0.60	TCs =27.92
Geldmacher et al., 2006	406 DR-7	Josephine N (Toblerone Ridge)	basalt	$^{40}Ar/^{39}Ar$ (StH)	mtrx	0.46	0.13	TCs =27.92
Geldmacher et al., 2006	407 DR-4	Josephine N (Pico Julia)	basalt	$^{40}Ar/^{39}Ar$ (StH)	mtrx	6.98	0.71	TCs =27.92
Geldmacher et al., 2006	407 DR-4	Josephine N (Pico Julia)	basalt	$^{40}Ar/^{39}Ar$ (StH)	mtrx	7.39	0.46	TCs =27.92
Geldmacher et al., 2006	408 DR-2	Josephine	basalt	$^{40}Ar/^{39}Ar$ (StH)	mtrx	15.84	0.86	TCs =27.92
Geldmacher et al., 2006	408 DR-2	Josephine	basalt	$^{40}Ar/^{39}Ar$ (StH)	mtrx	13.62	0.64	TCs =27.92
Geldmacher et al., 2006	409 DR-1	Josephine	basalt	$^{40}Ar/^{39}Ar$ (StH)	mtrx	11.58	0.72	TCs =27.92
Geldmacher et al., 2006	409 DR-1	Josephine	basalt	$^{40}Ar/^{39}Ar$ (StH)	mtrx	11.42	0.64	TCs =27.92
Geldmacher et al., 2006	410 DR-4	Josephine	basalt	$^{40}Ar/^{39}Ar$ (StH)	mtrx	13.15	0.62	TCs =27.92
Geldmacher et al., 2006	410 DR-4	Josephine	basalt	$^{40}Ar/^{39}Ar$ (StH)	mtrx	12.94	0.30	TCs =27.92
Wendt et al., 1976	9-101aKD	Josephine	basalt	K-Ar	mtrx	10.10	0.30	-
Wendt et al., 1976	9-101aKD	Josephine	basalt	K-Ar	mtrx	9.30	0.30	-
Wendt et al., 1976	9-123AT2	Josephine	basalt	K-Ar	mtrx	8.70	0.20	-
Wendt et al., 1976	9-123AT2	Josephine	basalt	K-Ar	mtrx	8.20	0.20	-
Wendt et al., 1976	9-123AT2	Josephine	basalt	K-Ar	mtrx	8.90	0.20	-
Wendt et al., 1976	9-123AT2	Josephine	basalt	K-Ar	mtrx	8.40	0.20	-
Wendt et al., 1976	9-127KD2	Josephine	basalt	K-Ar	mtrx	11.50	0.30	-
Wendt et al., 1976	9-127KD2	Josephine	basalt	K-Ar	mtrx	11.60	0.40	-
Wendt et al., 1976	9-133TD	Josephine	basalt	K-Ar	mtrx	9.60	0.40	-
Wendt et al., 1976	9-133TD	Josephine	basalt	K-Ar	mtrx	10.10	0.40	-
Wendt et al., 1976	9-133TD2	Josephine	basalt	K-Ar	mtrx	12.60	0.40	-
Wendt et al., 1976	9-133TD2	Josephine	basalt	K-Ar	mtrx	12.40	0.40	-
Merle et al., 2006	TMD16-1	Jo Sister/Erik	trachy-andesite	U-Pb (ID)	titanite	86.50	3.40	-
Merle et al., 2006	TMD16-2	Jo Sister/Erik	trachy-andesite	U-Pb (ID)	titanite	89.30	2.30	-
Geldmacher et al., 2006	412 DR-2	Jo Sister/Erik	basalt	$^{40}Ar/^{39}Ar$ (StH)	mtrx	3.62	0.32	TCs =27.92
Geldmacher et al., 2006	429 DR-1	Dragon	basalt	$^{40}Ar/^{39}Ar$ (StH)	mtrx	1.43	0.42	TCs =27.92
Geldmacher et al., 2006	429 DR-1	Dragon	basalt	$^{40}Ar/^{39}Ar$ (StH)	mtrx	1.12	0.20	TCs =27.92
Geldmacher et al., 2006	431 DR-1	Dragon	basalt	$^{40}Ar/^{39}Ar$ (StH)	mtrx	3.94	0.30	TCs =27.92
Geldmacher et al., 2007	428 DR-1	Godzilla	trachy-andesite	$^{40}Ar/^{39}Ar$ (TF)	hbl	66.20	0.50	TCs =27.92
Geldmacher et al., 2007	428 DR-1	Godzilla	trachy-andesite	$^{40}Ar/^{39}Ar$ (StH)	biot	66.69	0.17	TCs =27.92
Geldmacher et al., 2005	423 DR-1	Unicorn	basalt	$^{40}Ar/^{39}Ar$ (StH)	mtrx	27.40	2.40	TCs =27.92
Geldmacher et al., 2005	426 DR-1	Seine	basalt	$^{40}Ar/^{39}Ar$ (StH)	mtrx	21.70	0.20	TCs =27.92

ID: isotopic dilution; TF: total fusion; StH: step heating